EJN European Journal of Neuroscience

FENS Federation of European Neuroscience Societies

European Journal of Neuroscience, Vol. 47, pp. 399–416, 2018 doi:10.1111/ejn.13835

NEUROSYSTEMS

Predicting age from cortical structure across the lifespan

Christopher R. Madan[1,2] and Elizabeth A. Kensinger[2]
[1]School of Psychology, University of Nottingham, University Park, Nottingham NG7 2RD, UK
[2]Department of Psychology, Boston College, Chestnut Hill, MA, USA

Keywords: aging, brain morphology, cortical complexity, fractal dimensionality, gyrification, structural MRI

Abstract

Despite interindividual differences in cortical structure, cross-sectional and longitudinal studies have demonstrated a large degree of population-level consistency in age-related differences in brain morphology. This study assessed how accurately an individual's age could be predicted by estimates of cortical morphology, comparing a variety of structural measures, including thickness, gyrification and fractal dimensionality. Structural measures were calculated across up to seven different parcellation approaches, ranging from one region to 1000 regions. The age prediction framework was trained using morphological measures obtained from T1-weighted MRI volumes collected from multiple sites, yielding a training dataset of 1056 healthy adults, aged 18–97. Age predictions were calculated using a machine-learning approach that incorporated nonlinear differences over the lifespan. In two independent, held-out test samples, age predictions had a median error of 6–7 years. Age predictions were best when using a combination of cortical metrics, both thickness and fractal dimensionality. Overall, the results reveal that age-related differences in brain structure are systematic enough to enable reliable age prediction based on metrics of cortical morphology.

Introduction

It is well established that the structure of the brain changes as adults age—with decreases in cortical thickness as one of the most pronounced of these changes (e.g., Jernigan *et al.*, 2001; Salat *et al.*, 2004; Raz & Rodrigue, 2006; Fjell *et al.*, 2009, 2013; Hutton *et al.*, 2009; Lemaitre *et al.*, 2012; Hogstrom *et al.*, 2013; McKay *et al.*, 2014; Irimia *et al.*, 2015; Madan & Kensinger, 2016). However, other measures of cortical structure are also sensitive to age-related differences, such as gyrification (Magnotta *et al.*, 1999; Hogstrom *et al.*, 2013; Madan & Kensinger, 2016; Wang *et al.*, 2016; Cao *et al.*, 2017; Jockwitz *et al.*, 2017), which is a ratio of the regional surface area relative to the surface area of a simulated enclosing surface (Zilles *et al.*, 1988, 1989; Hofman, 1991; Armstrong *et al.*, 1995; Toro *et al.*, 2008; Kochunov *et al.*, 2012). More recently, a mathematical measure of the complexity of a structure, fractal dimensionality, has also been shown to index age-related differences in brain structure (Madan & Kensinger, 2016). While the use of fractal dimensionality with cortical aging is recent, it has been used in prior studies investigating differences in cortical structure in patient populations (Cook *et al.*, 1995; Free *et al.*, 1996; Thompson *et al.*, 2005; Sandu *et al.*, 2008; King *et al.*, 2009, 2010; Wu *et al.*, 2010; Nenadic *et al.*, 2014), as well as cross-species comparisons (Hofman, 1991). Importantly, age-related differences in these structural measures are not homogenous across the cortex; decreases in cortical thickness are most evident in frontal regions, while gyrification decreases primarily in parietal cortex. Given this, we wondered what degree of precision is useful in understanding age-related differences in cortical structure. Furthermore, it is unknown how well the relation between age and cortical structure metrics will generalize across independent samples. In this study, we sought to examine (1) the relative sensitivity of different cortical measures to age-related differences across the adult lifespan, (2) the granularity of these differences across different cortical parcellation approaches and (3) how well these different measures and parcellations can be used to *predict* age in independent samples. These findings should further our understanding of the neurobiological basis of healthy aging (Falk *et al.*, 2013; Reagh & Yassa, 2017).

Cortical metrics and granularity

While there is heterogeneity in age-related differences in cortical structure—for example, greater cortical thinning in frontal cortex than occipital (Sowell *et al.*, 2003; Salat *et al.*, 2004; Allen *et al.*, 2005; Fjell *et al.*, 2009; Hutton *et al.*, 2009; Hogstrom *et al.*, 2013)—it is unclear what degree of parcellation would be beneficial in characterizing healthy aging. Lobe-wise estimates of cortical thickness would likely be beneficial relative to overall mean cortical thickness, but would estimate for distinct gyri and lobules provide additional information? At some level of parcellation, additional predictive features should diminish, as cortical thickness between adjacent patches of cortex would be highly similar (within an individual).

Correspondence: Christopher R. Madan, as above. E-mail: christopher.madan@nottingham.ac.uk

Received 28 June 2017, revised 12 January 2018, accepted 15 January 2018

Edited by John Foxe. Reviewed by Rogier Kievit, University of Cambridge, UK; and Lars Ross, Albert Einstein College of Medicine, USA

All peer review communications can be found with the online version of the article.

Here, we investigated three measures of cortical structure—thickness, gyrification and fractal dimensionality. These measures were selected based on prior studies that had identified relationships between these measures and healthy aging, although these previous studies had used correlations rather than predictive models (e.g., Salat *et al.*, 2004; Fjell *et al.*, 2009; Hogstrom *et al.*, 2013; McKay *et al.*, 2014; Madan & Kensinger, 2016). This approach of using surface-based morphology allowed us to examine *distinct* measures of cortical structure. In particular, this is in contrast to voxel-based morphology (VBM) techniques which estimate gray matter volume and are influenced by a combination of structural features (Hutton *et al.*, 2009; Palaniyappan & Liddle, 2012; Fairchild *et al.*, 2015; Gerrits *et al.*, 2016). This point is made explicit by Mechelli *et al.* (2005), 'exactly the same differences would be detected when comparing images of thin, unfolded cortex against thin, folded cortex and thick, unfolded cortex' (see figure 5 of Mechelli *et al.*, 2005). As such, VBM is not sensitive to precise features as we sought to examine here, whereas surface-based morphometry captures these details unambiguously.

Many different approaches have been suggested to parcellate the human cortex (see Zilles & Amunts, 2010; for a review); here, we used seven parcellation approaches, focusing on atlases that have been implemented within FreeSurfer. The two standard parcellation atlases within FreeSurfer are the Desikan–Killiany–Tourville (DKT) atlas (Desikan *et al.*, 2006; Klein & Tourville, 2012) and the Destrieux atlas (Destrieux *et al.*, 2010), which divide the cortex into 62 and 148 parcellations, respectively. Both of these atlases define boundaries based on anatomical landmarks, with the main difference being that the Destrieux atlas divides gyri and sulci into separate parcellations, while the DKT atlas generally uses sulci as parcellation boundaries between gyri, as shown in Fig. 1. As two coarse atlases, we also considered the unparcellated cortical ribbon (i.e., only one region) as well as a lobe-wise parcellation (four regions). Supplementing the parcellation atlases standard within FreeSurfer, we also conducted analyses using structural metrics derived from three additional parcellation schemes: von Economo–Koskinas (86 regions; Scholtens *et al.*, 2018), Brainnetome (210 regions; Fan *et al.*, 2016), and Lausanne (1000 regions; Hagmann *et al.*, 2008). The von Economo–Koskinas

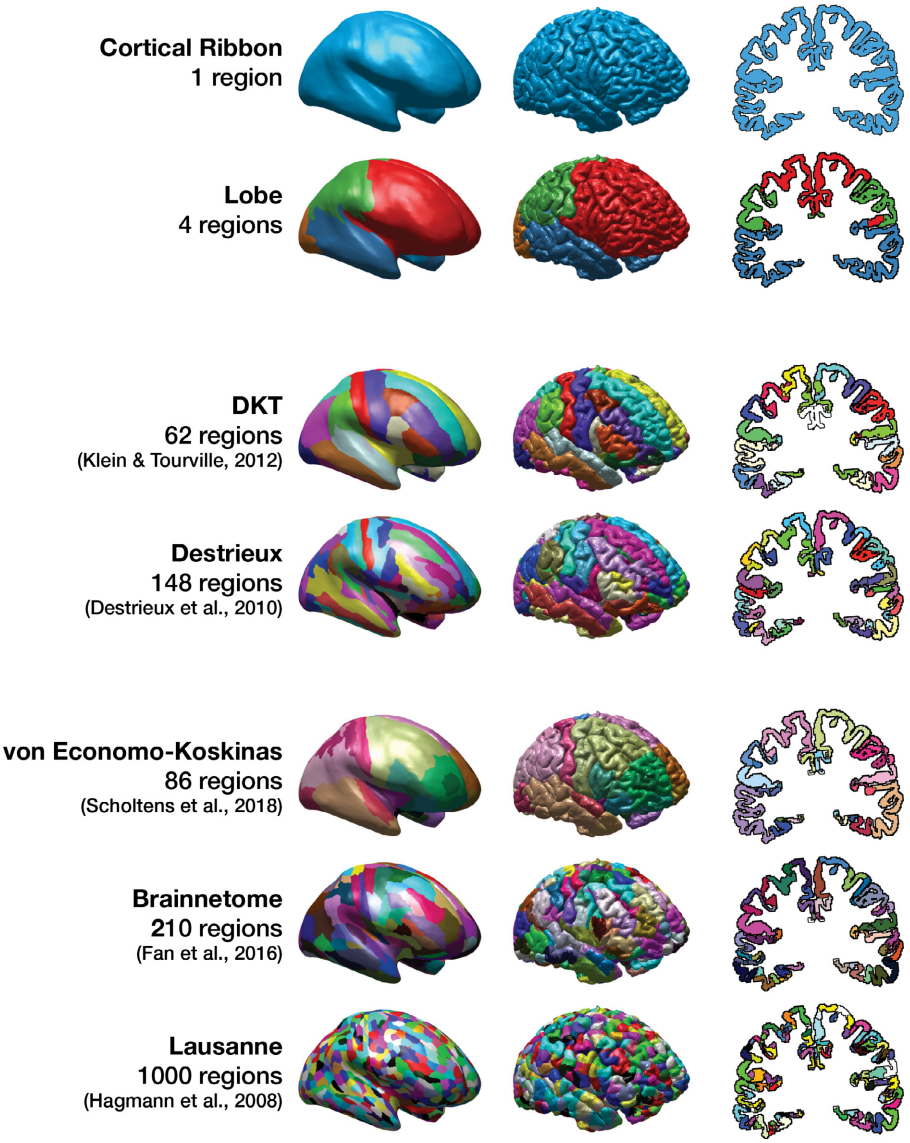

FIG. 1. Inflated and pial surfaces and an oblique coronal slice, from a young adult (20-year-old male), illustrating the seven parcellation approaches used. [Colour figure can be viewed at wileyonlinelibrary.com].

atlas was developed by Scholtens *et al.* (2018), based on the foundational work of von Economo & Koskinas (1925, 2008). This parcellation atlas is based on the cyctoarchitecture of the cortex [also see von Economo, 1927, 2009; previously some have used a hybrid approach to integrate von Economo's work with the Desikan–Killiany atlas (Scholtens *et al.*, 2015; van den Heuvel *et al.*, 2015)]. The Brainnetome atlas takes a different approach, using the Desikan–Killiany atlas and further parcellating it based on connectivity data from diffusion and resting-state scans (Fan *et al.*, 2016). The Lausanne atlas also initially starts from the Desikan–Killiany atlas and then further parcellates it into patches of approximately similar area (Hagmann *et al.*, 2008); here, we used the 1000 parcellation variant, although variants with less patches also exist. By predicting age in independent samples, across these different parcellation approaches, we can assess the cortical granularity of different structural metrics in relation to age-related differences in cortical structure.

While these parcellations are defined using anatomical landmarks, different parcellation approaches exist and it is unknown to what degree more discrete cortical parcellation regions—the topological granularity—will provide additional predictive value to inform the age prediction performance. It is also unknown whether some metrics of brain morphology would yield better prediction accuracy than others; the topology of age-related differences in thickness and gyrification has been shown to differ, and thus, they may be indicators of distinct aging processes (Hogstrom *et al.*, 2013; Madan & Kensinger, 2016). More recently, we have shown that measures of fractal dimensionality can show stronger age correlations than measures of cortical thickness and gyrification (Madan & Kensinger, 2016), but it was not known whether this would translate to additional predictive accuracy.

Predicting age from cortical measures

Although age-related differences in brain morphology are robust, there also can be extensive individual variability in the trajectory of brain aging (e.g., Pfefferbaum & Sullivan, 2015), and cross-sectional comparisons demonstrate that some older adults can have similar mean cortical thickness volumes as young adults (e.g., Salat *et al.*, 2004; Fjell *et al.*, 2009; Madan & Kensinger, 2016). In the absence of acquiring multiple MRI scans from the same individual, there are no methods that can easily discriminate among different age-related trajectories, nor is there agreement as to which metrics might be the best for identifying which individuals are likely to be on an accelerated-aging trajectory. This study took a first step by examining which parcellation techniques and estimates of cortical morphology would best *predict* an individual's age. Critically, here we measured the age predictions, rather than simply correlations with age, because significant relationships are not necessarily indicative of predictive value (e.g., see Lo *et al.*, 2015). As a further point of consideration, age-related differences in these metrics have been shown to be nonlinear (Fjell *et al.*, 2010, 2013), with age-related trajectories declining more steeply after 'critical ages' that also differ across structures (generally occurring between ages 40 and 70). Based on this evidence, we used a multiple smoothing spline-based regression procedure (Madan, 2016). Figure 2 shows representative cortical surfaces for individuals with ages in the first year of each decade, for each sex and training dataset used here. These cortical surfaces visibly show the degree of interindividual differences in cortical structure, but also make apparent the age-related differences in gyrification and sulcal width, along with other structural characteristics such as Yakovlevian torque. It is also visible here that male brains are generally slightly larger than female brains and that brain size tends to decrease with age. (Note that these are representative individual brains from the datasets used here, however, and not 'average' brains.)

Here, we sought to predict an individual's age from their brain morphology, attempting to optimize the brain parcellation and segmentation techniques so as to maximize their predictive accuracy. Although a few others have similarly sought to predict an individual's age from structural MRI volumes (e.g., Ashburner, 2007; Franke *et al.*, 2010, 2014; Franke & Gaser, 2012; Cole *et al.*, 2015; Schnack *et al.*, 2016; see Cole & Franke, 2017; for a review), these implementations relied on voxel-based morphometry (VBM) rather than regional surface-based morphology estimates and thus cannot be used to assess the predictive value of *specific* morphological features (e.g., thickness, gyrification) and cortical granularity as sought here. To construct this age prediction model, we used several open-access MRI datasets. The public sharing of MRI data has been quickly growing, and a large number of open-access datasets are now available (Biswal *et al.*, 2010; Mennes *et al.*, 2013; Poldrack & Gorgolewski, 2014; Das *et al.*, 2017; Madan, 2017; Poldrack *et al.*, 2017; Shenkin *et al.*, 2017). The use of open-access datasets enabled us to have the large sample sizes needed to have training datasets as well as held-out datasets, as well as demonstrate the generalizability and reproducibility of the presented results, although this was not possible only a few years ago (Dickie *et al.*, 2012).

Figure 3 provides an overview of factors that are known to influence estimates of brain morphology. These factors can be quite varied, ranging from transient changes, such as time-of-day (Nakamura *et al.*, 2015; Trefler *et al.*, 2016) and hydration (Duning *et al.*, 2005; Nakamura *et al.*, 2014), to more long-lasting changes, such as exercise (Hayes *et al.*, 2014; Steffener *et al.*, 2016), diet/lifestyle (Booth *et al.*, 2015; Khan *et al.*, 2015; Kullmann *et al.*, 2016) and meditation (Tang *et al.*, 2015). Brain morphology has also been linked with genetic variations, such as *APOE* and *BDNF* (see Strike *et al.*, 2015; for a comprehensive review). As such, it is important to acknowledge the breadth of effects that influence any measure of brain morphology. Although some of these sources of variability would be minimized if multiple scans were taken (e.g., at different times of day or with different levels of hydration), any model predicting an individual's age from *only* brain morphology estimates will be unable to account for some additional sources of variance and thus will have some degree of error. Nevertheless, it is useful to understand how well age predictions can be made on the basis of a structural scan that can be acquired in just a few minutes. Not only is this a relevant exercise for confirming the aspects of brain structure that are most strongly associated with age-associated differences, it also has potential clinical relevance; if the brain structure of healthy adults is a reasonable predictor of their age, then failures in age prediction (e.g., a structural scan that suggests someone is a decade older than they are) may help to indicate the presence of a prodromal state (Franke *et al.*, 2010, 2014; Franke & Gaser, 2012; Cole *et al.*, 2015; Schnack *et al.*, 2016; see Cole & Franke, 2017; for a review). While the current focus is on age-related differences through the adult lifespan, brain structure has also been examined through development (Dosenbach *et al.*, 2010; Brown *et al.*, 2012; Lee *et al.*, 2014; Qin *et al.*, 2015; Mills *et al.*, 2016; Somerville, 2016).

Procedure

Datasets

Three datasets were used to train the age prediction algorithm, with an additional two datasets used as independent test samples. The age distribution for each of the datasets is shown in Fig. 4.

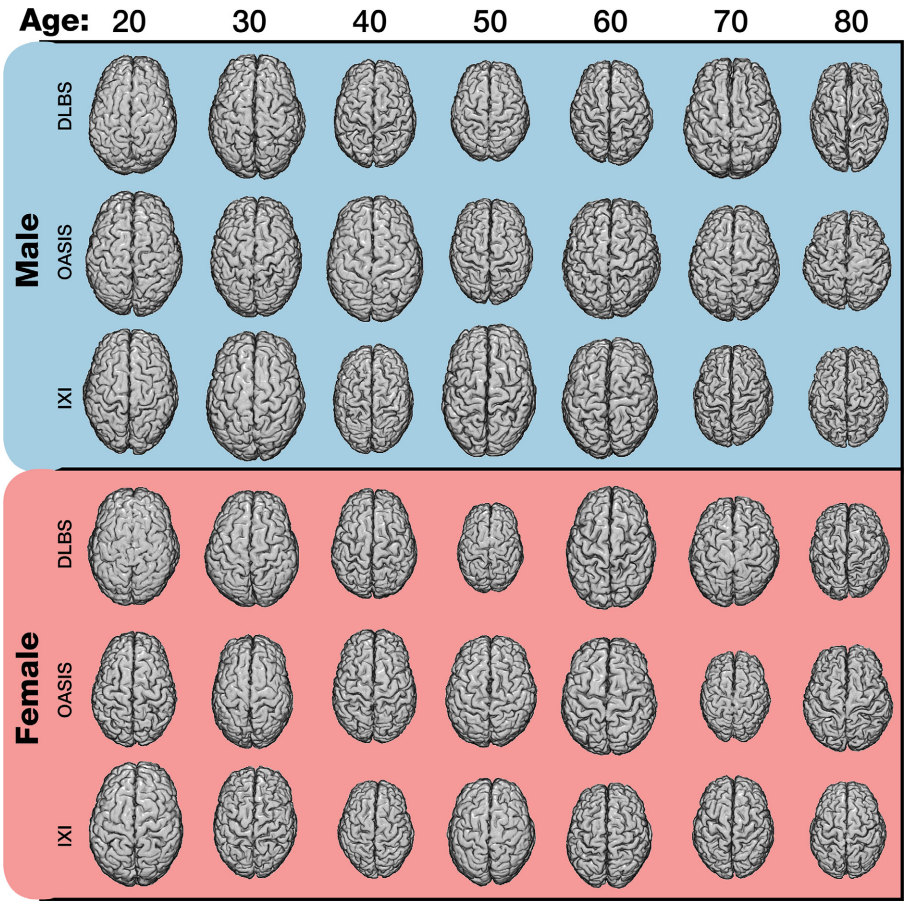

FIG. 2. Cortical surfaces for each age decade, sex, and training sample. Representative cortical surface reconstructions for individuals with ages in the first year of each decade (with the exception of 40 s, where there were insufficient male participants between ages 40 and 41). All reconstructions are shown at the same scale. 3D reconstruction images were generated as described in Madan (2015). [Colour figure can be viewed at wileyonlinelibrary.com].

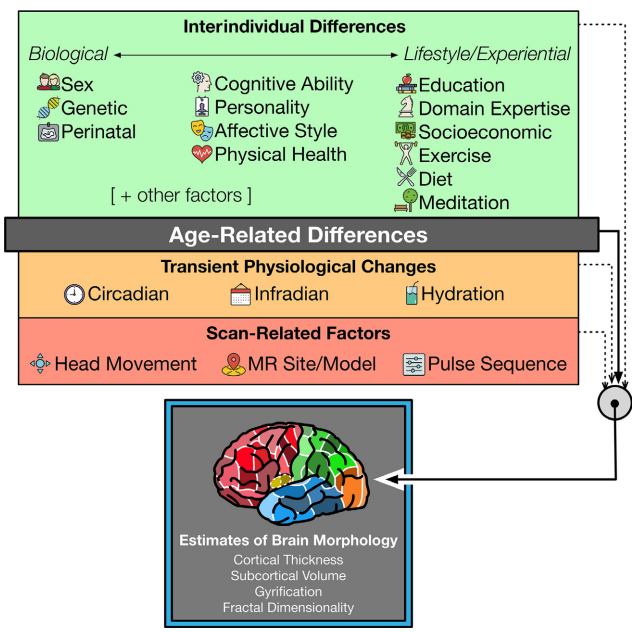

FIG. 3. Overview of factors known to influence estimates of brain morphology. [Colour figure can be viewed at wileyonlinelibrary.com].

Training Sample 1 (IXI) consisted of 427 healthy adults, (260 females) aged 20–86, from the publicly available Information eXtraction from Images (IXI) dataset (http://brain-development.org/ixi-dataset/). This is the same subset of individuals we used previously to investigate age-related differences in cortical regions; see Madan & Kensinger (2016, 2017a) for further details.

Training Sample 2 (OASIS) consisted of 314 healthy adults (196 females), aged 18–94, from the publicly available Open Access Series of Imaging Studies (OASIS) cross-sectional dataset (Marcus *et al.*, 2007; http://www.oasis-brains.org). Participants were screened for neurological and psychiatric issues; the Mini-Mental State Examination (MMSE) and Clinical Dementia Rating (CDR) were administered to participants aged 60 and older. In the current sample, participants with a CDR above zero were excluded; all remaining participants scored 25 or above on the MMSE. Multiple T1 volumes were acquired using a Siemens Vision 1.5 T with a MPRAGE sequence; only the first volume was used here. Scan parameters were as follows: TR = 9.7 ms; TE = 4.0 ms; flip angle = 10°; voxel size = 1.25 × 1×1 mm. This sample was previously used in Madan & Kensinger (2017a) and Madan (2018).

Training Sample 3 (DLBS) consisted of 315 healthy adults (198 females), aged 20–89, from wave 1 of the Dallas Lifespan Brain Study (DLBS), made available through the International Neuroimaging Data-sharing Initiative (INDI; Mennes *et al.*, 2013) and hosted on the Neuroimaging Informatics Tools and Resources

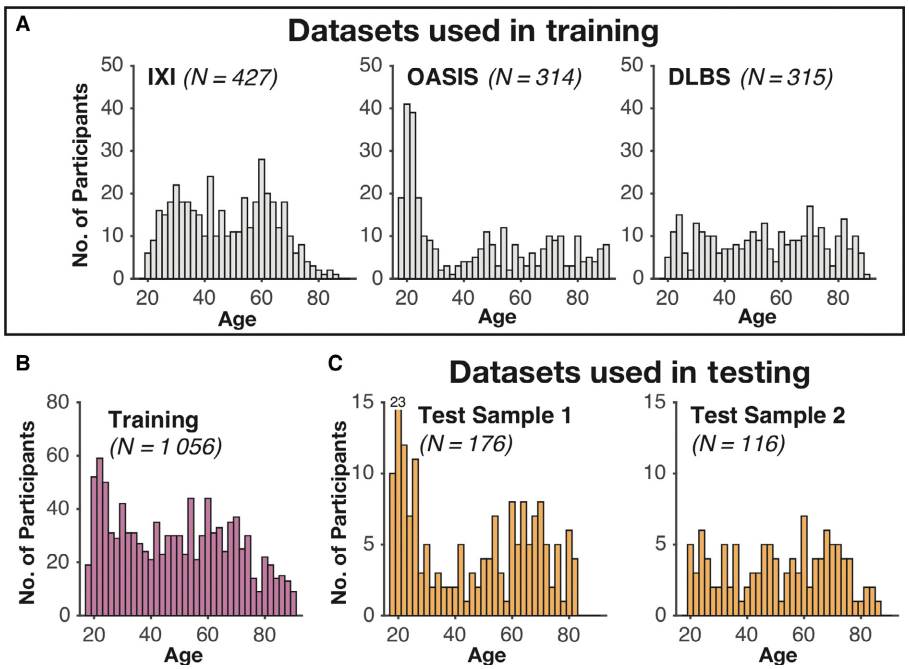

FIG. 4. Age distributions for each of the datasets. (A) Age distributions for each of the datasets used in the training. (B) Age distribution for the aggregated training dataset (i.e., combining IXI, OASIS, and DLBS). (C) Age distributions for the independent test datasets. [Colour figure can be viewed at wileyonlinelibrary.com].

Clearinghouse (NITRC; Kennedy *et al.*, 2016) (http://fcon_1000.projects.nitrc.org/indi/retro/dlbs.html). Participants were screened for neurological and psychiatric issues. All participants scored 26 or above on the MMSE. T1 volumes were acquired using a Philips Achieva 3 T with a MPRAGE sequence. Scan parameters were as follows: TR = 8.1 ms; TE = 3.7 ms; flip angle = 12°; voxel size = 1 × 1×1 mm. See Kennedy *et al.* (2015) and Chan *et al.* (2014) for further details about the dataset; this sample was previously used in Madan (2018).

Test Sample 1 consisted of 176 healthy adults (89 females), aged 18–83, recruited by the Cognitive and Affective Laboratory at Boston College (BC) and screened for neurological and psychiatric issues, and to have scored above 26 on the MMSE. T1 volumes were acquired using a Siemens Trio 3 T with a MEMPRAGE sequence optimized for morphometry studies (van den Heuvel *et al.*, 2008; Wonderlick *et al.*, 2009). Scan parameters were as follows: TR = 2530 ms; TE = 1.64, 3.50, 5.36, 7.22 ms; flip angle = 7°; voxel size = 1 × 1×1 mm. This sample was previously used in Madan & Kensinger (2017a).

Test Sample 2 consisted of 116 healthy adults (70 females), aged 20–87, recruited by Dr. Craig Stark's laboratory at University of California–Irvine (UCI) and screened for neurological and psychiatric issues, and to have scored above 26 on the MMSE, made available on NITRC (Kennedy *et al.*, 2016) (https://www.nitrc.org/projects/stark_aging/). T1 volumes were acquired using a Philips Achieva 3 T with a MPRAGE sequence. Scan parameters were as follows: TR = 11 ms; TE = 4.6 ms; flip angle = 12°; voxel size = 0.75 × 0.75 × 0.75 mm. See Stark *et al.* (2013) and Bennett *et al.* (2015) for further details about the dataset.

Pre-processing of the structural MRIs

Data were analyzed using FreeSurfer v.5.3.0 (https://surfer.nmr.mgh.harvard.edu) on a machine running CentOS 6.6. FreeSurfer was used to automatically volumetrically segment and parcellate cortex from the T1-weighted images (Dale *et al.*, 1999; Fischl *et al.*, 1999, 2002, 2004; Fischl & Dale, 2000; Fischl, 2012). FreeSurfer's standard pipeline was used (i.e., `recon-all`), and no manual edits were made to the surface meshes. Cortical thickness is calculated as the distance between the white matter surface (white–gray interface) and pial surface (gray–CSF interface) (Dale *et al.*, 1999; Fischl & Dale, 2000). Thickness estimates have previously been found to be in agreement with manual measurements from MRI images (Kuperberg *et al.*, 2003; Salat *et al.*, 2004), as well as *ex vivo* tissue measurements (Rosas *et al.*, 2002; Cardinale *et al.*, 2014). Gyrification was calculated using FreeSurfer, as described in Schaer *et al.* (2012).

Cortical parcellations

Here, we used seven parcellation atlases to determine the amount of relevant age-related differences in cortical structure: (1) entire cortical ribbon (one region; i.e., unparcellated); (2) each of the four lobes (four regions); (3) DKT atlas (62 regions; Klein & Tourville, 2012); (4) Destrieux *et al.* (2010) atlas (148 regions); (5) von Economo–Koskinas atlas (86 regions; Scholtens *et al.*, 2018); (6) Brainnetome atlas (210 regions; Fan *et al.*, 2016); and (7) Lausanne atlas (1000 regions; Hagmann *et al.*, 2008). Each of these parcellation approaches is shown in Fig. 1. The DKT and Destrieux atlases are included as standard parcellation atlases within FreeSurfer. The lobe parcellation was delineated by grouping parcellation regions from the Destrieux atlas, as done in Madan & Kensinger (2016).

The von Economo–Koskinas, Brainnetome and Lausanne atlases were applied to each individual's reconstructed cortical surface using `mris_ca_label` with the cortical parcellation atlas files (`*.gcs`) that have been distributed online by the respective researchers. The von Economo–Koskinas atlas was implemented in

FreeSurfer by Scholtens *et al.* (2018; http://www.dutchconnectomelab.nl/economo/), based on the cortical areas identified by von Economo & Koskinas (1925). The Brainnetome atlas was developed by Fan *et al.* (2016; http://atlas.brainnetome.org) based on a modified Desikan–Killiany atlas (Desikan *et al.*, 2006; a precursor to the DKT atlas) that initially reduced the number of cortical regions to 20 per hemisphere (rather than the 34) but then further parcellated the cortex using connectivity data extracted from diffusion and resting-state scans, resulting in a total of 210 regions. The Lausanne atlas was similarly initially constructed using the Desikan–Killiany atlas and then further subdivided each region into smaller patches of approximately equivalent area (Hagmann *et al.*, 2008). The Lausanne atlas is distributed as part of the Connectome Mapper (Daducci *et al.*, 2012; https://github.com/LTS5/cmp).

Fractal dimensionality

The complexity of each structure was calculated using as the fractal dimensionality of the filled structure. Our work previously demonstrated that fractal dimensionality indexes age-related differences in cortical and subcortical structures better than extant measures (i.e., cortical thickness, cortical gyrification, subcortical volume), where older adults exhibit reductions in structural complexity relative to younger adults (Madan & Kensinger, 2016, 2017a; Madan, 2018). In fractal geometry, several approaches have been proposed to quantify the 'dimensionality' or complexity of a fractal; the approach here calculates the Minkowski–Bouligand or Hausdorff dimension (see Mandelbrot, 1967). This structural property can be measured by considering the 3D structure within a grid space and counting the number of boxes that overlap with the edge of the structure. By then using another grid size (i.e., changing the box width), the relationship between the grid size and number of counted boxes can be determined ('box-counting algorithm'). Here, we used box sizes (in mm) corresponding to powers of 2, ranging from 0 to 4 (i.e., 2^k [where $k = \{0, 1, 2, 3, 4\}$] = 1, 2, 4, 8, 16 mm). The slope of this relationship in log-log space is the fractal dimensionality of the structure. Thus, the corresponding equation is:

$$\mathrm{FD} = -\frac{\Delta \log_2(\mathrm{Count})}{\Delta \log_2(\mathrm{Size})}$$

If only the boxes overlapping with the edge/surface of the structure are counted, this slope represents the fractal dimensionality of the *surface* (FD_s). If the boxes within the structure are additionally counted, the resulting slope represents the fractal dimensionality of the *filled* volume (FD_f; see Fig. 5). As the relative alignment of the grid space and the structure can influence the obtained fractal dimensionality value using the box-counting algorithm, we instead used a dilation algorithm that is equivalent to using a sliding grid space and calculating the fractal dimensionality at each alignment (Madan & Kensinger, 2016, 2017b).

Fractal dimensionality was calculated using the calcFD toolbox (Madan & Kensinger, 2016; http://cmadan.github.io/calcFD/). Briefly, the toolbox calculates the 'fractal dimensionality' of a 3D structure and is designed to use intermediate files from the standard FreeSurfer analysis pipeline. calcFD was first applied to measure the complexity of the cortical ribbon and lobes (Madan & Kensinger, 2016), but has been extended to subcortical structures (Madan & Kensinger, 2017a; Madan, 2018), and the DKT parcellation atlas (Madan & Kensinger, 2017b).

Here, we only used the fractal dimensionality of the filled structures (FD_f), as this measure has been demonstrated to be more sensitive, than the fractal dimensionality of the surface, to age-related differences in cortical structure (Madan & Kensinger, 2016). For each participant, the fractal dimensionality was calculated for (a) entire cortical ribbon (one region); (b) four lobes (four regions); (c) DKT-parcellated atlas (62 regions); and (d) von Economo–Koskinas atlas (86 regions). As smaller parcellations of cortex inherently have decreased fractal dimensionality, that is, becoming closer to a truncated rectangular pyramid, we did not calculate the fractal dimensionality for the parcellation atlases with smaller regions (see Fig. 1)

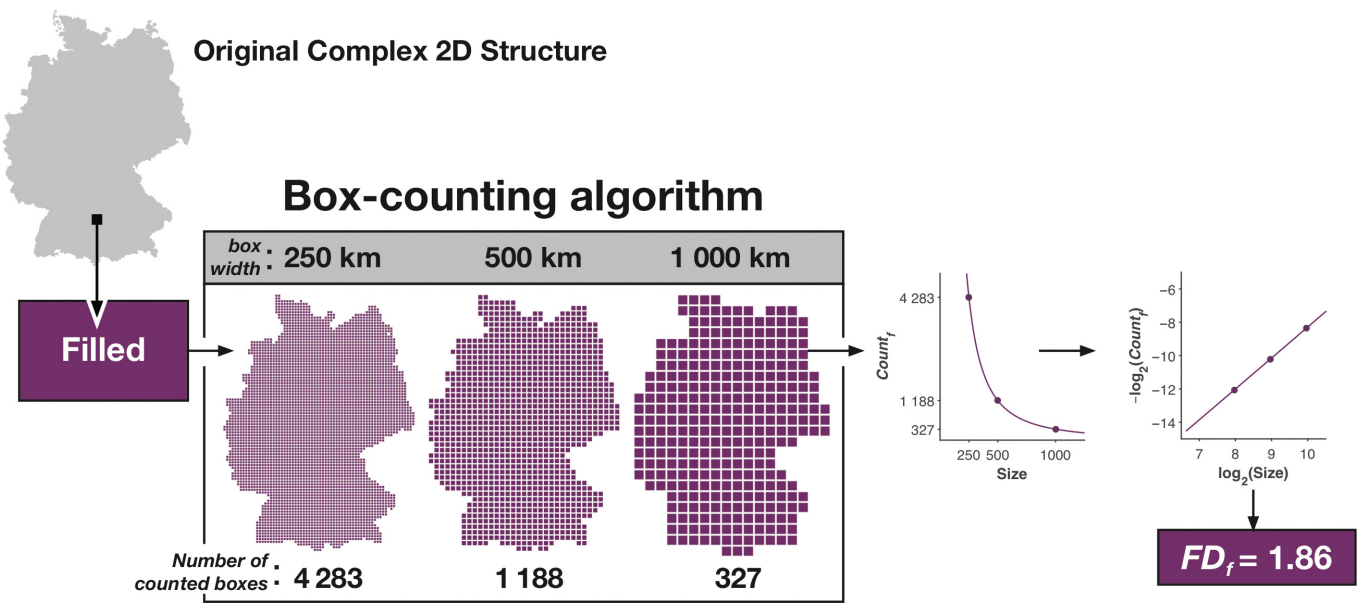

FIG. 5. Illustration of how fractal dimensionality is measured from a 2D structure. Modified from Madan and Kensinger (2016). [Colour figure can be viewed at wileyonlinelibrary.com].

(Madan & Kensinger, 2017a,b). Indeed, prior analyses indicated that the parcellations in the Destrieux atlas were too fine-grained for meaningful fractal dimensionality calculations but that the regions within the DKT atlas were of sufficient size (Madan & Kensinger, 2017b).

Age prediction algorithm

A machine-learning approach was used to predict age (in years) from brain morphology. Specifically, we trained a machine-learning regression framework with the aggregated training data ($N = 1056$), using brain morphology data to predict the age data. We then applied the trained regression model to the brain morphology data from the test samples to obtain age predictions. Age predictions were then compared with the actual age data. Performance of the age predictions was evaluated using two metrics: R^2 and *MdAE*. R^2 was used as a measure of explained variability. Median absolute error (*MdAE*) has been found to be more robust to outliers than mean squared error (*MSE*) (Armstrong & Collopy, 1992; Hyndman & Koehler, 2006).

The machine-learning regression framework primarily relies on several statistical methods to minimize over-fitting through regularization, dimensionality reduction and feature selection. This is accomplished through sequentially applying three statistical techniques: smoothing spline regression, PCA and relevance vector regression (RVR)—which we have implemented as a MATLAB toolbox called Prism (Madan, 2016). These statistical techniques are described further below. As a whole, Prism is a MATLAB toolbox designed for conducting spline-based multiple regression using training and test datasets. Benchmark analyses indicated that Prism provided better age prediction estimates than standard RVR (Madan, 2016). Prism was configured to (a) use least-squares splines to reduce over-fitting (smoothness parameter set to 0.1) and (b) keep the principal components that explained the most variance, retaining as many components as necessary to explain 95% of the variance. Values were *Z*-scored prior to the smoothing spline regression to ensure that different measures were smoothed to the same degree, as the smoothness parameter is influenced by the overall magnitude of the input values (as in Madan, 2018).

Relevance Vector Regression (RVR)

To make predictions using the structural measures, we employed relevance vector regression (RVR). RVR is the application of relevance vector machine or RVM to a regression problem and is a relatively recent machine-learning technique (Tipping, 2000, 2001; Tipping & Faul, 2003). In functionality, RVM shares many characteristics with support vector machines (SVM), but is generally more flexible (Tipping, 2000). RVM can also be considered as a special case of a Sparse Bayesian framework (Tipping, 2001; Tipping & Faul, 2003) or Gaussian process (Rasmussen & Williams, 2006). For a more in-depth discussion of RVM, see Bishop (2006).

Broadly, RVR is similar to multiple linear regression with regularization (e.g., LASSO and ridge regression; see Tibshirani, 1996; Hastie *et al.*, 2009), which reduces the number of predictors/model complexity by removing those predictors that are redundant, reducing over-fitting and yielding a more generalizable model. The implementation of this procedure is sometimes referred to as automatic relevance determination (ARD) (MacKay, 1996; Wipf & Nagarajan, 2007). Further, it has been suggested that RVR is comparable to a Bayesian implementation of LASSO regression (Park & Casella, 2008; Gao *et al.*, 2010; Jamil & ter Braak, 2012). Here, we used the MATLAB implementation of RVM that uses an accelerated training algorithm (Tipping & Faul, 2003), freely available from the author's website (http://www.miketipping.com/sparsebayes.htm).

Smoothing spline regression

While age-related changes in morphology are often modeled using linear and quadratic functions (e.g., Sowell *et al.*, 2003; Walhovd *et al.*, 2011; Hogstrom *et al.*, 2013; Madan & Kensinger, 2016), nonlinear functions have been shown to better model age-related differences (Fjell *et al.*, 2010, 2013). This approach uses smoothing spline regression, where the relationship between a predictor and dependent variable is fit using piece-wise cubic functions (Wahba & Wold, 1975; Wahba, 1990; Fox, 2000). Cubic smoothing spline is implemented in MATLAB as the function `csaps`. Here, each predictor (i.e., brain morphology measure) was treated as an independent predictor of age and was individually regressed vs. age. To combine these estimates, that is, for multiple regression, the Prism toolbox was used (Madan, 2016).

Held-out test data

Age prediction performance here was evaluated using independent test datasets. This approach was taken to ensure that the age predictions were not biased—for instance, numerous studies have demonstrated that performance with *k*-fold cross-validation can lead to over-fitting in the model selection (e.g., Golbraikh & Tropsha, 2002; Rao *et al.*, 2008; Saeb *et al.*, 2016; Skocik *et al.*, 2016).

Pre- and post-processing

Data were maintained as three separate datasets: training, test sample 1 and test sample 2. Within each dataset, main effects of sex were initially regressed out before being entered into the machine-learning regression framework; the main effect of site was also regressed out for the training dataset. Outputted age predictions were mean centered (to the mean of the predicted ages) to compensate for sample differences (as in Franke *et al.*, 2010; Franke & Gaser, 2012). The variance in the predicted ages in the test data was also matched to variance of the training data, to correct for a regression-to-the-mean bias.

Results

Regional age-related differences in cortical structure

In our prior work investigating age-related differences in cortical structure (Madan & Kensinger, 2016), we had only used bilateral lobe parcellations (i.e., four regions). However, in subsequent work, our fractal dimensionality analyses were used with the DKT parcellation, with 62 cortical parcellations (Madan & Kensinger, 2017b). While we use this improved parcellation method in the current paper, along with multiple regression methods to estimate age predictions in held-out test samples, we thought it would be useful to calculate the relationship between structural measures for each parcellation with age.

We used a smoothing spline regression approach, as described in the methods, with the full training dataset ($N = 1056$). All of the regressions controlled for effects of site.

We first conducted smoothing spline regressions using the cortical ribbon measures. Interindividual differences in mean cortical thickness explained 47.17% of the variance in age (i.e., R^2). Mean

TABLE 1. Summary of age prediction model performance

			Test sample 1						Test sample 2					
			Percentiles						Percentiles					
Parcellation	Measure	# Regions	10th	25th	50th	75th	90th	R^2	10th	25th	50th	75th	90th	R^2
Ribbon	Thickness	1	2.3	4.2	8.7	16.9	27.7	.54	2.5	8.1	14.9	20.2	27.9	.36
	Gyrification	1	1.1	4.3	9.8	17.4	24.8	.54	2.9	6.4	10.7	18.6	26.9	.45
	FD	1	1.7	3.1	5.6	11.8	17.8	.76	1.3	4.4	8.7	14.8	22.1	.64
	Combined	3	1.0	2.7	6.9	10.9	20.1	.74	1.6	5.8	8.6	15.6	21.0	.61
Lobe	Thickness	4	1.8	3.7	8.8	15.9	27.0	.50	3.7	7.9	12.5	21.6	29.9	.35
	Gyrification	4	1.5	4.7	9.3	17.8	24.3	.56	2.5	6.4	11.6	17.1	24.9	.50
	FD	4	1.0	3.0	6.5	12.7	16.5	.77	1.8	3.2	6.8	14.3	20.7	.71
	Combined	12	0.8	2.9	7.0	10.3	18.1	.79	1.4	2.6	7.9	15.1	18.3	.71
DKT	Thickness	62	1.7	4.2	8.9	15.3	24.1	.59	4.0	7.3	10.6	18.4	24.1	.52
	Gyrification	62	2.1	3.8	8.6	18.1	21.6	.62	2.6	4.2	7.2	15.3	23.5	.49
	FD	62	1.8	3.5	7.7	13.9	18.9	.67	2.7	5.2	11.6	16.5	22.7	.54
	Combined	186	1.0	3.0	5.9	10.3	15.1	.81	2.7	4.3	7.3	14.4	16.5	.69
von Economo–Koskinas	Thickness	86	2.4	3.8	8.2	13.6	21.5	.65	3.6	7.4	11.0	18.9	22.2	.49
	Gyrification	86	1.6	4.0	7.2	18.2	23.8	.58	3.0	5.6	9.6	16.5	22.4	.52
	FD	86	1.4	4.0	7.7	12.6	18.6	.76	2.3	4.6	9.2	16.3	21.4	.59
	Combined	258	1.3	2.6	5.7	10.0	12.8	.85	1.6	3.6	8.5	12.0	14.4	.76
Destrieux	Thickness	148	1.4	4.0	8.2	12.3	19.7	.71	1.1	2.9	8.5	16.2	23.9	.52
	Gyrification	148	1.7	4.0	9.9	17.0	21.5	.61	2.9	4.9	10.8	14.9	22.2	.49
Brainnetome	Thickness	210	1.5	3.1	7.9	13.6	19.7	.68	1.5	6.4	9.9	16.3	21.4	.57
Lausanne	Thickness	1000	0.7	2.9	8.4	12.8	18.5	.73	1.4	5.5	9.9	13.6	18.5	.67
Thickness (Brainnetome) + FD (Lobe)		214	1.0	2.7	**6.1**	9.8	17.0	**.80**	1.3	2.9	**7.5**	13.2	18.8	**.72**

Median and R^2 values for the best-fitting model are shown in bold.

gyrification explained 36.07% of the variance; fractal dimensionality (of the filled volume) explained 73.53% of the variance. Reassuringly, these values correspond reasonably well with the variances explained in the independent, held-out test samples (see Table 1). For comparison, with linear and quadratic effects in the IXI sample alone, these values were 33.55, 20.61 and 51.66%, respectively (as reported in Madan & Kensinger, 2016); the relative increases in the explained variance correspond to the use of spline regression, instead of linear and quadratic regression, and also indicate that our overall approach and between-site harmonization was successful.

We subsequently conducted similar smoothing spline regressions for each of the 62 cortical parcellations of the DKT atlas, as shown in Fig. 6A. The cortical thickness and gyrification analyses correspond well with the comparable analysis by Hogstrom *et al.* (2013). Age-related differences in cortical thickness are most pronounced in frontal regions and the superior temporal gyrus, and are least effected in occipital regions, the superior parietal lobule and the postcentral gyrus. In contrast, age-related differences in gyrification are most pronounced in the pre- and postcentral gyri, caudal middle frontal gyrus, as well as supramaginal gyrus and inferior parietal lobule. Frontal regions and parcellations on the medial surface have the least age-related differences in gyrification.

Age-related differences in fractal dimensionality have a topology that resembles a mixture of the thickness and gyrification patterns, but is generally higher in explained variance (i.e., R^2). Regional fractal dimensionality was most affected by age in the superior temporal gyrus and inferior parietal lobule, although frontal regions were also markedly affected. Interindividual differences in fractal dimensionality of the inferior temporal gyrus and regions along the medial surface were the least associated with age.

As shown in Fig. 6B, we also conducted a similar analysis using the von Economo–Koskinas atlas (Scholtens *et al.*, 2018) and found a similar pattern of results across the parcellations and cortical measures. Figure 6C shows that the most age-sensitive regions from the other atlases generalize to the Brainnetome atlas as well; however, thickness of many parcellations are only weakly related to age, likely due to the substantially smaller regions here and an increasing role of interindividual differences and regional specificity.

Age prediction models

To investigate the relationship between brain morphology and age-prediction performance, we first calculated a benchmark measure and then compared age prediction models using regional cortical thickness for each of the seven parcellation approaches. Next, we compared different structural measures (i.e., thickness, gyrification, fractal dimensionality and a combination of all three) across four parcellation atlases. Finally, we took a theoretical approach to combining the morphological measures to best capture age-related differences in structure. Results from the age prediction models are summarized in Table 1.

Benchmark performance

To provide a benchmark to evaluate the age prediction performance in the held-out test data using the various estimates of brain morphology, a simple estimation of a lower-bound (shown in light gray in Fig. 7) was determined by 'predicting' that all participants' ages in the test dataset were the mean of the dataset. As such, $R^2 = 0$ for this benchmark model, and we would not expect any reasonable age prediction model to produce worse estimates than this.

In Fig. 7, each box-and-whisker denotes the median (i.e., *MdAE*) as a tick mark. The box spans the 25th to 75th percentiles; the whiskers span the 10th to 90th percentiles.

Cortical thickness

Performance for the age prediction models based on cortical thickness, for each of the seven parcellation approaches, is shown in Fig. 7 and Table 1. Results show that finer-grain parcellations

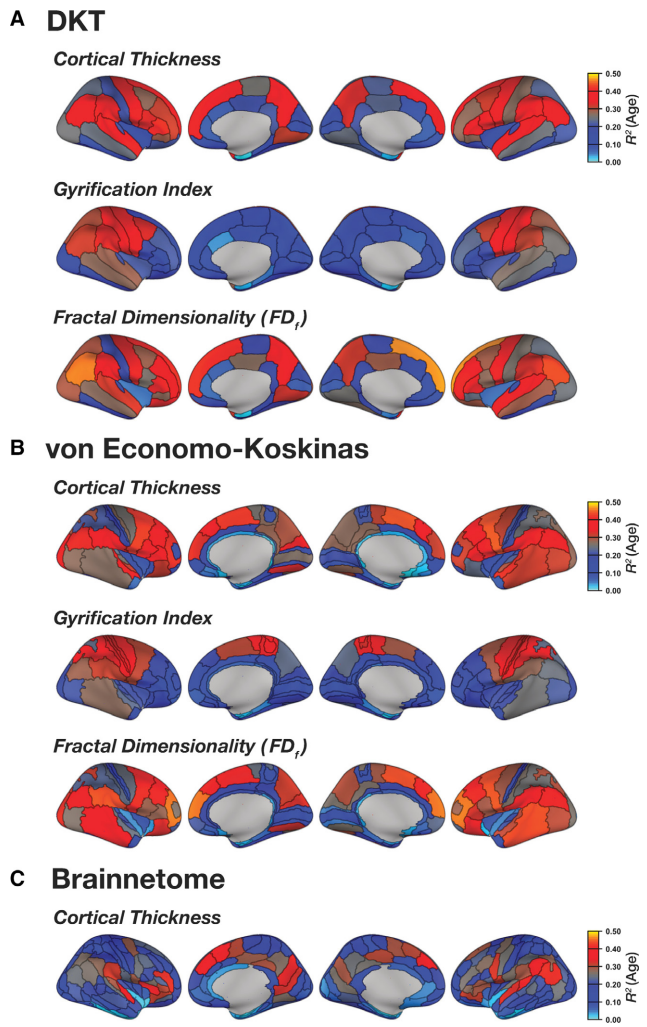

FIG. 6. Regional age-prediction differences (R^2) using the (A) DKT, (B) von Economo-Koskinas atlases, and (C) Brainnetome for the respective structural measures using smoothing-spline regression. [Colour figure can be viewed at wileyonlinelibrary.com].

generally yielded better age predictions, demonstrating that regional heterogeneity in age-related differences in cortical thickness led to improved prediction performance. Age prediction models using the cortical ribbon and lobe parcellations performed comparably, indicating that the slight increase in heterogeneity with the lobe parcellations was not sufficient to improve predictions. However, performance on the atlases that had more fine-grain parcellations led to a decrease in the median absolute error of approximately 3 years. Performance between these different atlases did not markedly differ, with age predictions having a median error of 7–10 years. While performance with the Lausanne atlas (which comprised 1000 regions) was relatively good, it was not better than the parcellation atlases that had far fewer regions. Here, we considered the Brainnetome atlas to be the best performing model based on cortical thickness estimates.

Comparing different measures of morphology

Next, we compared age prediction models based on cortical thickness, gyrification and fractal dimensionality. As indicated earlier, fractal dimensionality inherently becomes less sensitive with smaller parcellations and was only used for the cortical parcellations with < 100 regions.

Beginning with models using only a single value for the unparcellated cortical ribbon, the model based on the fractal dimensionality did markedly better than those based on mean cortical thickness or gyrification. Combining the three measures (i.e., three predictors in the regression) led to worse age predictions than complexity alone, due to insufficient feature selection and/or possible over-fitting. Given that there were only three predictors input, this suggests that the automatic relevance determination used in RVR was not 'strict' enough to only use complexity, although later combined models were able to perform better than their component models that relied on only a single measure of morphology. The age prediction models using the lobe-wise parcellation scheme performed relatively similarly to those that only used the cortical ribbon.

The models that used the DKT parcellation atlas using only one of the morphology measures performed comparably to those with the unparcellated ribbon and lobe parcellations; however, the combined model here did perform notably better. The combined model had a median error of 8 years and R^2 values near .70. As noted earlier, age predictions based on cortical thickness improved markedly when using the DKT parcellation, relative to the ribbon and lobe parcellations. Importantly, we also found that the fractal dimensionality model using the DKT parcellation was performing worse than the ribbon and lobe models, suggesting that using the finer-grain parcellations was resulting to notable losses in complexity-related information, as alluded to previously. Interestingly, the age prediction models based on the von Economo–Koskinas atlas performed comparably with the DKT atlas when each structural metric was used independently, but error was sufficiently lower when the metrics were combined.

Combining measures

The four combined models are shown in orange in Fig. 7. Based on the performance of these age prediction models, we constructed an additional model, combining the two best cortical measures, across different parcellation approaches—cortical thickness from the regions of the Brainnetome parcellation atlas, and fractal dimensionality from the lobe-wise parcellation. This newly constructed model (shown in light green) out-performed the component models, indicating that the two structural measures each provided unique age-related difference characteristics. A scatter plot of the predicted and actual ages for this model is shown in Fig. 8.

Discussion

The present study reveals that interindividual differences in cortical structure are not only strongly correlated with age, but also can robustly be used to predict age. Although almost any metric of cortical structure can predict age to within a decade (10–12 years), the present study also reveals that by optimizing metrics, a much more accurate prediction (6–7 years) can be achieved. In-line with prior results (Hogstrom *et al.*, 2013; Madan & Kensinger, 2016), we found that differences in gyrification are not as related to age as cortical thickness, and fractal dimensionality was a better morphological metric of age-related differences than either of these other metrics. Importantly, the best age predictions were achieved when both fractal dimensionality and cortical thickness were combined, demonstrating that these metrics contribute unique information about age-related differences in brain structure.

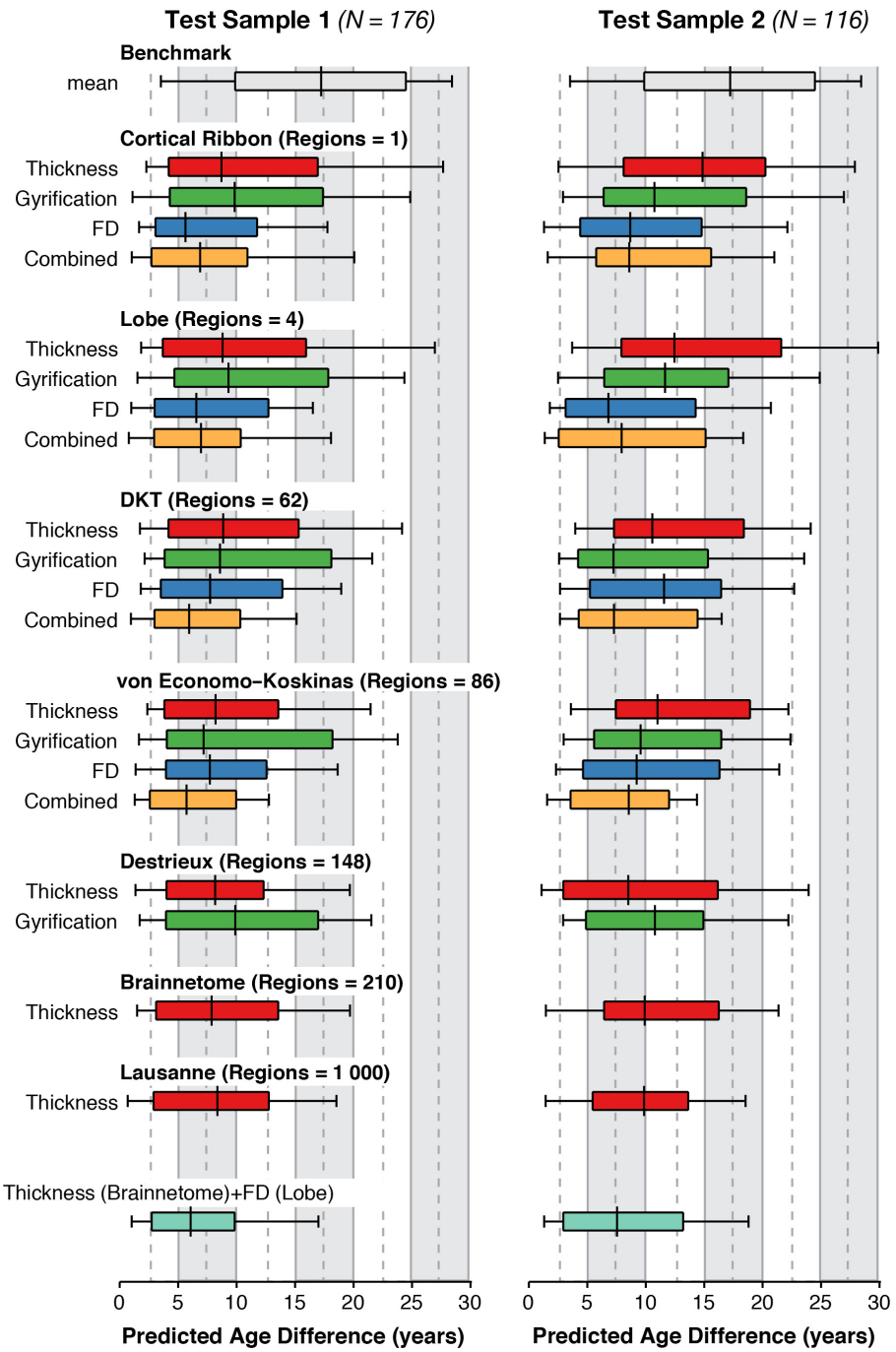

FIG. 7. Age-prediction performance for the models based on each of parcellation atlases and structural measures. '*Regions*' corresponds to the number of regions/predictors used in the model (see Figure 1). *'FD'* denotes fractal dimensionality of the filled structures. Each box-andwhisker bar denotes the median (i.e., *MdAE*) as a tick-mark. The box spans the 25th to 75th percentiles; the whiskers span the 10th to 90th percentiles. Values for each of these percentiles, as well as R^2, are reported in Table 1. [Colour figure can be viewed at wileyonlinelibrary.com].

Across different cortical parcellation schemes, cortical thickness estimates localized to different gyri and sulci are substantially more indicative of age-related differences relative to lobe-wise measurement. The recently developed Brainnetome atlas was selected as the best atlas for representing age-related differences in cortical thickness, although the DKT, Destrieux and von Economo–Koskinas atlases did not markedly differ in performance. Parcellating the cortex into even more constrained patches (i.e., the Lausanne atlas) did not provide any additional predictive value, indicating that the level morphological granularity in the Brainnetome parcellation was sufficient for age predictions based on cortical thickness estimates. Fractal dimensionality inherently becomes less sensitive with smaller parcellations and performed best when only using lobe-wise parcellations, rather than the more fine-grained parcellations of the DKT and von Economo–Koskinas atlases. Gyrification did not appear to be sufficiently predictive of age to further contribute to predictions.

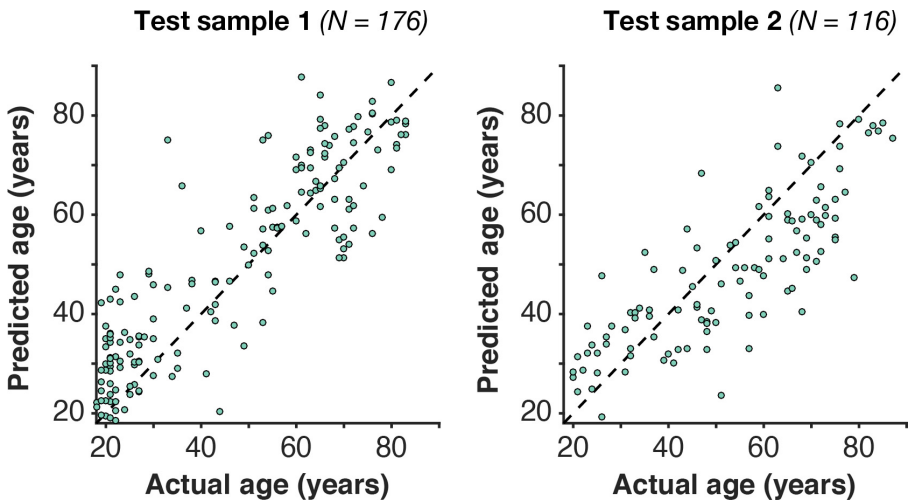

FIG. 8. Scatter plot of the actual and predicted age for the best-fitting model. [Colour figure can be viewed at wileyonlinelibrary.com].

Without pooling across different atlases, the von Economo–Koskinas atlas produced relatively good age predictions when the three cortical metrics were combined.

Within the broader literature, the age prediction approach here can serve as a baseline model of healthy, successful aging. For instance, this approach can be used to characterize which regions exhibit more or less age-related variability. As the training and test datasets were wholly independent, age predictions applied to additional independent datasets should be indicative of healthy aging. Future studies could use the current approach with smaller samples, where larger differences between predicted age and chronological age would be indicative of cohort characteristics related to atypical aging. Of course, it would still be optimal to have MRI data for 'healthy' individuals acquired alongside the group of interest to account for differences related to scanner hardware, pulse sequence or potential differences in demographics (e.g., years of education).

Although the present results reveal systematic age-related differences in brain structure, several questions remain about the nature of these age differences. For instance, the cortical measures used here are limited to macroscopic differences, as differences in the microstructure (e.g., neuron density, neuropil composition) are beyond the capabilities of current MRI methods. This raises the question of what neurobiological changes are manifesting in these macroscopic changes in structure. In a different vein, in models where age predictions performed relatively poorer, and in light of the myriad of ways that individual brains can differ, one must wonder what other non-aging factors may be manifesting in morphological differences and minimizing the ability to isolate age differences. In the following two sections, we outline the extant literature that investigates these two topics.

Neurobiological basis of age-related differences in brain structure

While a large number of studies examining age-related differences in cortical thickness have found reduced cortical thickness in older adults, particularly in frontal regions, the underlying changes in the cortical microstructure are unclear (Sowell *et al.*, 2003; Koo *et al.*, 2012; Dickstein *et al.*, 2013; Meyer *et al.*, 2014). One reason this has yet to be resolved is that to do so appropriately would require not only MRI data but also postmortem histological tissue samples. Extant histological evidence suggests that age-related differences in cortical regions are generally not associated with a decrease in the number or size of neurons (Morrison & Hof, 1997; Peters *et al.*, 1998; Uylings & de Brabander, 2002; Peters & Rosene, 2003; Freeman *et al.*, 2008; Gefen *et al.*, 2015; von Bartheld, 2017), despite initial suggestions to the contrary (Terry *et al.*, 1987). What does appear to differ, however, is the dendritic structure, particularly in pyramidal neurons, as well as other features of the neuropil (Scheibel *et al.*, 1975; Peters, 2002; Uylings & de Brabander, 2002; Duan *et al.*, 2003; Eickhoff *et al.*, 2005; Dickstein *et al.*, 2007, 2013; Hao *et al.*, 2007; Casanova *et al.*, 2011; Morrison & Baxter, 2012). Convergently, pyramidal neurons are particularly prominent in prefrontal cortex, as well as prefrontal pyramidal neurons having orders of magnitude more dendritic spines than those in some other regions (Elston, 2003).

The literature investigating the biological basis for age-related differences in gyrification is even more sparse. Unlike cortical thickness, age-related differences in gyrification are most pronounced in the parietal lobe (Hogstrom *et al.*, 2013; Madan & Kensinger, 2016). In a large sample of chimpanzees, Autrey *et al.* (2014) observed increased gyrification in adults relative to adolescents, consistent with human data; however, an age-related decrease in gyrification was not observed. The authors thus attributed the age-related decrease in gyrification in humans as a being related to the extended lifespan of humans, although many other factors also may be relevant (e.g., exercise and diet).

Non-aging factors that influence brain morphology

While the goal of the current work was to examine the relationship between age and brain morphology, a multitude of other factors is also known to influence estimates of brain morphology. Broadly, these other factors can be categorized as follows: (1) interindividual differences; (2) transient physiological changes; and (3) scan-related factors, as outlined in Fig. 3. Here, we only included age as a predictor and did not include these additional factors, and thus, prediction accuracy was inherently limited; however, future work including some of these factors should yield more precise predictions. Furthermore, an important next step will be to examine the relative contribution of different interindividual difference measures to age prediction performance.

Interindividual differences in morphology can arise from many sources, including biological and lifestyle/experiential factors. It is

well established that there are sex differences in brain morphology (Barnes *et al.*, 2010; Herron *et al.*, 2015; Hutton *et al.*, 2009; McKay *et al.*, 2014; Potvin *et al.*, 2016; Salat *et al.*, 2004; Sowell *et al.*, 2007). Brain morphology has also been linked with genetic variations; even in healthy individuals, genetic variants of *APOE* (Donix *et al.*, 2010; Honea *et al.*, 2010; Okonkwo *et al.*, 2012; Reinvang *et al.*, 2013; Mormino *et al.*, 2014; Riedel *et al.*, 2016) and *BDNF* (Nemoto *et al.*, 2006; Pezawas *et al.*, 2004; but see Harrisberger *et al.*, 2014) relate to brain morphology estimates. Factors related to perinatal development such as birth weight and nutrition are also associated with morphology, during development and through to adulthood (Walhovd *et al.*, 2012, 2014, 2016; Strømmen *et al.*, 2015). Other lifestyle and experiential factors also can influence brain morphology. Expertise within specific domains has been associated with regional differences in morphology (see May, 2011; for a review), such as in chess players (Hänggi *et al.*, 2014), taxi drivers (Maguire *et al.*, 2000), musicians (Tervaniemi, 2009), athletes (Tseng *et al.*, 2013; Schlaffke *et al.*, 2014) and video game players (Erickson *et al.*, 2010; Kühn *et al.*, 2013). Morphological changes can also arise from experiences such as meditation (Tang *et al.*, 2015; Luders *et al.*, 2016) or from a lack of normal experience, as in acquired blindness (Li *et al.*, 2017). Other important interindividual factors lay somewhere on a continuum in-between biological and lifestyle. Physical health factors, such as exercise and diet, can also influence brain morphology (Hayes *et al.*, 2014; Booth *et al.*, 2015; Khan *et al.*, 2015; Fletcher *et al.*, 2016; Kullmann *et al.*, 2016; Steffener *et al.*, 2016; Williams *et al.*, 2017). Interindividual differences such as cognitive abilities, personality and affective style are also associated with morphological differences (Bjørnebekk *et al.*, 2013; Kievit *et al.*, 2014; Holmes *et al.*, 2016; Yamagishi *et al.*, 2016; Gignac & Bates, 2017; Riccelli *et al.*, 2017; Valk *et al.*, 2017). A growing literature has also demonstrated relationships between socioeconomic status and brain morphology (Hanson *et al.*, 2013; Brito & Noble, 2014; Piccolo *et al.*, 2016; Brito *et al.*, 2017; LeWinn *et al.*, 2017).

Beyond interindividual differences in morphology, transient physiological effects can also influence estimates of brain morphology and likely also estimates of test–retest reliability. These changes include time-of-day effects (Nakamura *et al.*, 2015; Trefler *et al.*, 2016) and structural changes over the course of longer periods (i.e., infradian), such as the menstrual cycle (Hagemann *et al.*, 2011; Protopopescu *et al.*, 2008; Ossewaarde *et al.*, 2013; Lisofsky *et al.*, 2015). Hydration can also influence brain morphometry (Duning *et al.*, 2005; Kempton *et al.*, 2009; Nakamura *et al.*, 2014; Streitbürger *et al.*, 2012; but see Meyers *et al.*, 2016).

Scan-related effects can affect estimates of morphology, without an actual change in morphology. For instance, head movement during scan acquisition can lead to decreased estimates of cortical thickness (Reuter *et al.*, 2015; Alexander-Bloch *et al.*, 2016; Pardoe *et al.*, 2016; Savalia *et al.*, 2017). Effects of head movement on morphology estimates are particularly relevant here, as there is evidence that older adults tend to move more during scanning than younger adults (Andrews-Hanna *et al.*, 2007; Van Dijk *et al.*, 2012; Salat, 2014; Savalia *et al.*, 2017; but see preliminary evidence that fractal dimensionality may be robust to head movement, Madan & Kensinger, 2016). Differences in pulse sequence, magnetic field strength and other interscanner effects can also influence estimates of morphology (Han *et al.*, 2006; Jovicich *et al.*, 2009, 2013; Wonderlick *et al.*, 2009; Lüsebrink *et al.*, 2013; Iscan *et al.*, 2015; Potvin *et al.*, 2016; Madan & Kensinger, 2017b; Erus *et al.*, 2018; Fortin *et al.*, 2018; Zaretskaya *et al.*, 2018), as well as software packages, and even versions, used for data analysis (Chepkoeck *et al.*, 2016; Glatard *et al.*, 2015; Gronenschild *et al.*, 2012; Johnson *et al.*, 2017).

In sum, estimates of brain morphology are subject to many sources of variability that are often not considered, with future studies necessary to further our understanding of the complex interplay among these factors.

Future directions

Prediction accuracy may be improved by extending it to multimodal protocols. For instance, other imaging techniques have been found to index age-related differences, such as iron content (Bartzokis *et al.*, 1994; Zecca *et al.*, 2004; Callaghan *et al.*, 2014; Ward *et al.*, 2014; Daugherty & Raz, 2015; Ghadery *et al.*, 2015; Acosta-Cabronero *et al.*, 2016), white matter tract integrity (Gunning-Dixon *et al.*, 2009; Lebel *et al.*, 2012; Chen *et al.*, 2013; Teipel *et al.*, 2014; Bender *et al.*, 2016; Cox *et al.*, 2016; Kodiweera *et al.*, 2016), and arterial-spin labeling (Chen *et al.*, 2013). Functional connectivity (e.g., from resting-state fMRI data) could also be used to complement the current approach (e.g., Dosenbach *et al.*, 2010; Qin *et al.*, 2015; Geerligs & Tsvetanov, 2016; Liem *et al.*, 2017). Other non-imaging measures, such as lifestyle factors (e.g., diet, smoking, vascular health, education and exercise) or blood biomarkers. may also improve prediction accuracy (Geerligs & Tsvetanov, 2016; Madsen *et al.*, 2016).

Future work can take advantage of this framework to compare relative differences in 'brain age' associated with different participant samples, both healthy and patient populations. For instance, prior studies have found evidence suggesting overestimated aging predictions in patients with Alzheimer's disease (Franke & Gaser, 2012), traumatic brain injuries (Cole *et al.*, 2015) and schizophrenia (Schnack *et al.*, 2016). Other individuals, such as long-term meditation practitioners, have been found to have significantly underestimated age predictions (Luders *et al.*, 2016).

Conclusion

Here, we demonstrate that reliable age predictions can be made from structural MRI volumes. A combination of cortical thickness and fractal dimensionality yields the best predictions. The present framework may also prove useful for future research contrasting healthy aging relative to samples of participants exhibiting pathological aging or superagers, as well as for investigating other sources of variability within healthy older adults (such as cognition-, lifestyle- or health-related factors).

Acknowledgements

Portions of this research were supported by a grant from the National Institutes of Health (MH080833; to E.A.K.) and by funding provided by Boston College. C.R.M. was supported by a fellowship from the Canadian Institutes of Health Research (FRN-146793).

MRI data used in the preparation of this article were obtained from several sources, and data were provided in part by (1) the Open Access Series of Imaging Studies (OASIS; Marcus *et al.*, 2007); (2) the Information eXtraction from Images (IXI) dataset (funded by Engineering and Physical Sciences Research Council [EPSRC] of the UK [EPSRC GR/S21533/02]); (3) wave 1 of the Dallas Lifespan Brain Study (DLBS) led by Dr. Denise Park and distributed through INDI (Mennes *et al.*, 2013) and NITRC (Kennedy *et al.*, 2016); (4) the BC data were acquired with the support of funding from the Searle Foundation, the McKnight Foundation and the National Institutes of Mental Health; and (5) cross-sectional aging data acquired by Dr. Craig Stark's laboratory at University of California–Irvine and distributed through NITRC.

Conflict of interest

The authors have no conflict of interests to disclose.

Author contributions

C.R.M. conceived the study design, conducted the data analyses and drafted the manuscript. E.A.K. contributed to the study design and provided critical feedback on the manuscript. Both authors approved the final version of the manuscript.

Data accessibility

Details on accessing the datasets used here are described in the Datasets section.

Abbreviations

DKT, Desikan–Killiany–Tourville; FD, fractal dimensionality; fMRI, functional magnetic resonance imaging; MdAE, median absolute error; MRI, magnetic resonance imaging; PCA, principal component analysis; RVR, relevance vector regression.

References

Acosta-Cabronero, J., Betts, M.J., Cardenas-Blanco, A., Yang, S. & Nestor, P.J. (2016) *In vivo* MRI mapping of brain iron deposition across the adult lifespan. *J. Neurosci.*, **36**, 364–374.

Alexander-Bloch, A., Clasen, L., Stockman, M., Ronan, L., Lalonde, F., Giedd, J. & Raznahan, A. (2016) Subtle in-scanner motion biases automated measurement of brain anatomy from *in vivo* MRI. *Hum. Brain Mapp.*, **37**, 2385–2397.

Allen, J.S., Bruss, J., Brown, C.K. & Damasio, H. (2005) Normal neuroanatomical variation due to age: the major lobes and a parcellation of the temporal region. *Neurobiol. Aging*, **26**, 1245–1260.

Andrews-Hanna, J.R., Snyder, A.Z., Vincent, J.L., Lustig, C., Head, D., Raichle, M.E. & Buckner, R.L. (2007) Disruption of large-scale brain systems in advanced aging. *Neuron*, **56**, 924–935.

Armstrong, J.S. & Collopy, F. (1992) Error measures for generalizing about forecasting methods: empirical comparisons. *Int. J. Forecasting*, **8**, 69–80.

Armstrong, E., Schleicher, A., Omran, H., Curtis, M. & Zilles, K. (1995) The ontogeny of human gyrification. *Cereb. Cortex*, **5**, 56–63.

Ashburner, J. (2007) A fast diffeomorphic image registration algorithm. *NeuroImage*, **38**, 95–113.

Autrey, M.M., Reamer, L.A., Mareno, M.C., Sherwood, C.C., Herndon, J.G., Preuss, T., Schapiro, S.J. & Hopkins, W.D. (2014) Age-related effects in the neocortical organization of chimpanzees: gray and white matter volume, cortical thickness, and gyrification. *NeuroImage*, **101**, 59–67.

Barnes, J., Ridgway, G.R., Bartlett, J., Henley, S.M.D., Lehmann, M., Hobbs, N., Clarkson, M.J., MacManus, D.G. *et al.* (2010) Head size, age and gender adjustment in MRI studies: a necessary nuisance? *NeuroImage*, **53**, 1244–1255.

von Bartheld, C.S. (2017) Myths and truths about the cellular composition of the human brain: a review of influential concepts. *J. Chem. Neuroanat.* doi: 10.1016/j.jchemneu.2017.08.004. [Epub ahead of print]

Bartzokis, G., Mintz, J., Sultzer, D., Marx, P., Herzberg, J.S., Phelan, C.K. & Marder, S.R. (1994) *In vivo* MR evaluation of age-related increases in brain iron. *Am. J. Neuroradiol.*, **15**, 1129–1138.

Bender, A.R., Völkle, M.C. & Raz, N. (2016) Differential aging of cerebral white matter in middle-aged and older adults: a seven-year follow-up. *NeuroImage*, **125**, 74–83.

Bennett, I.J., Huffman, D.J. & Stark, C.E.L. (2015) Limbic tract integrity contributes to pattern separation performance across the lifespan. *Cereb. Cortex*, **25**, 2988–2999.

Bishop, C.M. (2006) *Pattern Recognition and Machine Learning*. Springer, New York.

Biswal, B.B., Mennes, M., Zuo, X.-N., Gohel, S., Kelly, C., Smith, S.M., Beckmann, C.F., Adelstein, J.S. *et al.* (2010) Toward discovery science of human brain function. *Proc. Natl. Acad. Sci. USA*, **107**, 4734–4739.

Bjørnebekk, A., Fjell, A.M., Walhovd, K.B., Grydeland, H., Torgersen, S. & Westlye, L.T. (2013) Neuronal correlates of the five factor model (FFM) of human personality: multimodal imaging in a large healthy sample. *NeuroImage*, **65**, 194–208.

Booth, T., Royle, N.A., Corley, J., Gow, A.J., del C. Valdés Hernández, M., Maniega, S.M., Ritchie, S.J., Bastin, M.E. *et al.* (2015) Association of allostatic load with brain structure and cognitive ability in later life. *Neurobiol. Aging*, **36**, 1390–1399.

Brito, N.H. & Noble, K.G. (2014) Socioeconomic status and structural brain development. *Front. Neurosci.*, **8**, 276.

Brito, N.H., Piccolo, L.R. & Noble, K.G. (2017) Associations between cortical thickness and neurocognitive skills during childhood vary by family socioeconomic factors. *Brain Cogn.*, **116**, 54–62.

Brown, T.T., Kuperman, J.M., Chung, Y., Erhart, M., McCabe, C., Hagler, D.J., Venkatraman, V.K., Akshoomoff, N. *et al.* (2012) Neuroanatomical assessment of biological maturity. *Curr. Biol.*, **22**, 1693–1698.

Callaghan, M.F., Helms, G., Lutti, A., Mohammadi, S. & Weiskopf, N. (2014) A general linear relaxometry model of R1 using imaging data. *Magn. Reson. Med.*, **73**, 1309–1314.

Cao, B., Mwangi, B., Passos, I.C., Wu, M.-J., Keser, Z., Zunta-Soares, G.B., Xu, D., Hasan, K.M. *et al.* (2017) Lifespan gyrification trajectories of human brain in healthy individuals and patients with major psychiatric disorders. *Sci. Rep.*, **7**, 511.

Cardinale, F., Chinnici, G., Bramerio, M., Mai, R., Sartori, I., Cossu, M., Russo, G.L., Castana, L. *et al.* (2014) Validation of FreeSurfer-estimated brain cortical thickness: comparison with histologic measurements. *Neuroinformatics*, **12**, 535–542.

Casanova, M.F., El-Baz, A. & Switala, A. (2011) Laws of conservation as related to brain growth, aging, and evolution: symmetry of the minicolumn. *Front. Neuroanat.*, **5**, 66.

Chan, M.Y., Park, D.C., Savalia, N.K., Petersen, S.E. & Wig, G.S. (2014) Decreased segregation of brain systems across the healthy adult lifespan. *Proc. Natl. Acad. Sci. USA*, **111**, E4997–E5006.

Chen, J.J., Rosas, H.D. & Salat, D.H. (2013) The relationship between cortical blood flow and sub-cortical white-matter health across the adult age span. *PLoS One*, **8**, e56733.

Chepkoeck, J.-L., Walhovd, K.B., Grydeland, H. & Fjell, A.M. (2016) Effects of change in FreeSurfer version on classification accuracy of patients with Alzheimer's disease and mild cognitive impairment. *Hum. Brain Mapp.*, **37**, 1831–1841.

Cole, J.H. & Franke, K. (2017) Predicting age using neuroimaging: innovative brain ageing biomarkers. *Trends Neurosci.*, **40**, 681–690.

Cole, J.H., Leech, R. & Sharp, D.J. (2015) Prediction of brain age suggests accelerated atrophy after traumatic brain injury. *Ann. Neurol.*, **77**, 571–581.

Cook, M.J., Free, S.L., Manford, M.R.A., Fish, D.R., Shorvon, S.D. & Stevens, J.M. (1995) Fractal description of cerebral cortical patterns in frontal lobe epilepsy. *Eur. Neurol.*, **35**, 327–335.

Cox, S.R., Ritchie, S.J., Tucker-Drob, E.M., Liewald, D.C., Hagenaars, S.P., Davies, G., Wardlaw, J.M., Gale, C.R. *et al.* (2016) Ageing and brain white matter structure in 3,513 UK Biobank participants. *Nat. Commun.*, **7**, 13629.

Daducci, A., Gerhard, S., Griffa, A., Lemkaddem, A., Cammoun, L., Gigandet, X., Meuli, R., Hagmann, P. *et al.* (2012) The Connectome Mapper: an open-source processing pipeline to map connectomes with MRI. *PLoS One*, **7**, e48121.

Dale, A.M., Fischl, B. & Sereno, M.I. (1999) Cortical surface-based analysis: I. Segmentation and surface reconstruction. *NeuroImage*, **9**, 179–194.

Das, S., Glatard, T., Rogers, C., Saigle, J., Paiva, S., MacIntyre, L., Safi-Harab, M., Rousseau, M.-E. *et al.* (2017) Cyberinfrastructure for open science at the Montreal Neurological Institute. *Front Neuroinform.*, **10**, 53.

Daugherty, A.M. & Raz, N. (2015) Appraising the role of iron in brain aging and cognition: promises and limitations of MRI methods. *Neuropsychol. Rev.*, **25**, 272–287.

Desikan, R.S., Ségonne, F., Fischl, B., Quinn, B.T., Dickerson, B.C., Blacker, D., Buckner, R.L., Dale, A.M. *et al.* (2006) An automated labeling system for subdividing the human cerebral cortex on MRI scans into gyral based regions of interest. *NeuroImage*, **31**, 968–980.

Destrieux, C., Fischl, B., Dale, A. & Halgren, E. (2010) Automatic parcellation of human cortical gyri and sulci using standard anatomical nomenclature. *NeuroImage*, **53**, 1–15.

Dickie, D.A., Job, D.E., Poole, I., Ahearn, T.S., Staff, R.T., Murray, A.D. & Wardlaw, J.M. (2012) Do brain image databanks support understanding of normal ageing brain structure? A systematic review. *Eur. Radiol.*, **22**, 1385–1394.

Dickstein, D.L., Kabaso, D., Rocher, A.B., Luebke, J.I., Wearne, S.L. & Hof, P.R. (2007) Changes in the structural complexity of the aged brain. *Aging Cell*, **6**, 275–284.

Dickstein, D.L., Weaver, C.M., Luebke, J.I. & Hof, P.R. (2013) Dendritic spine changes associated with normal aging. *Neuroscience*, **251**, 21–32.
Donix, M., Burggren, A.C., Suthana, N.A., Siddarth, P., Ekstrom, A.D., Krupa, A.K., Jones, M., Rao, A. *et al.* (2010) Longitudinal changes in medial temporal cortical thickness in normal subjects with the APOE-4 polymorphism. *NeuroImage*, **53**, 37–43.
Dosenbach, N.U.F., Nardos, B., Cohen, A.L., Fair, D.A., Power, J.D., Church, J.A., Nelson, S.M., Wig, G.S. *et al.* (2010) Prediction of individual brain maturity using fMRI. *Science*, **329**, 1358–1361.
Duan, H., Wearne, S.L., Rocher, A.B., Macedo, A., Morrison, J.H. & Hof, P.R. (2003) Age-related dendritic and spine changes in corticocortically projecting neurons in macaque monkeys. *Cereb. Cortex*, **13**, 950–961.
Duning, T., Kloska, S., Steinstrater, O., Kugel, H., Heindel, W. & Knecht, S. (2005) Dehydration confounds the assessment of brain atrophy. *Neurology*, **64**, 548–550.
von Economo, C.F. (1927) *Zellaufbau der Grosshirnrinde des Menschen*. Springer, Berlin.
von Economo, C.F. (2009) *Cellular Structure of the Human Cerebral Cortex*. Karger, Basel.
von Economo, C.F. & Koskinas, G.N. (1925) *Die cytoarchitektonik der hirnrinde des erwachsenen menschen*. Springer, Berlin.
von Economo, C.F. & Koskinas, G.N. (2008) *Atlas of Cytoarchitectonics of the Adult Human Cerebral Cortex*. Karger, Basel.
Eickhoff, S., Walters, N.B., Schleicher, A., Kril, J., Egan, G.F., Zilles, K., Watson, J.D.G. & Amunts, K. (2005) High-resolution MRI reflects myeloarchitecture and cytoarchitecture of human cerebral cortex. *Hum. Brain Mapp.*, **24**, 206–215.
Elston, G.N. (2003) Cortex, cognition and the cell: new insights into the pyramidal neuron and prefrontal function. *Cereb. Cortex*, **13**, 1124–1138.
Erickson, K.I., Boot, W.R., Basak, C., Neider, M.B., Prakash, R.S., Voss, M.W., Graybiel, A.M., Simons, D.J. *et al.* (2010) Striatal volume predicts level of video game skill acquisition. *Cereb. Cortex*, **20**, 2522–2530.
Erus, G., Doshi, J., An, Y., Verganelakis, D., Resnick, S.M. & Davatzikos, C. (2018) Longitudinally and inter-site consistent multi-atlas based parcellation of brain anatomy using harmonized atlases. *NeuroImage*, **166**, 71–78.
Fairchild, G., Toschi, N., Hagan, C.C., Goodyer, I.M., Calder, A.J. & Passamonti, L. (2015) Cortical thickness, surface area, and folding alterations in male youths with conduct disorder and varying levels of callous–unemotional traits. *Neuroimage Clin.*, **8**, 253–260.
Falk, E.B., Hyde, L.W., Mitchell, C., Faul, J., Gonzalez, R., Heitzeg, M.M., Keating, D.P., Langa, K.M. *et al.* (2013) What is a representative brain? Neuroscience meets population science. *Proc. Natl. Acad. Sci. USA*, **110**, 17615–17622.
Fan, L., Li, H., Zhuo, J., Zhang, Y., Wang, J., Chen, L., Yang, Z., Chu, C. *et al.* (2016) The Human Brainnetome Atlas: a new brain atlas based on connectional architecture. *Cereb. Cortex*, **26**, 3508–3526.
Fischl, B. (2012) FreeSurfer. *NeuroImage*, **62**, 774–781.
Fischl, B. & Dale, A.M. (2000) Measuring the thickness of the human cerebral cortex from magnetic resonance images. *Proc. Natl. Acad. Sci. USA*, **97**, 11050–11055.
Fischl, B., Sereno, M.I. & Dale, A.M. (1999) Cortical surface-based analysis: II. Inflation, flattening, and a surface-based coordinate system. *NeuroImage*, **9**, 195–207.
Fischl, B., Salat, D.H., Busa, E., Albert, M., Dieterich, M., Haselgrove, C., van der Kouwe, A., Killiany, R. *et al.* (2002) Whole brain segmentation: automated labeling of neuroanatomical structures in the human brain. *Neuron*, **33**, 341–355.
Fischl, B., Salat, D.H., van der Kouwe, A.J.W., Makris, N., Ségonne, F., Quinn, B.T. & Dale, A.M. (2004) Sequence-independent segmentation of magnetic resonance images. *NeuroImage*, **23**, S69–S84.
Fjell, A.M., Westlye, L.T., Amlien, I., Espeseth, T., Reinvang, I., Raz, N., Agartz, I., Salat, D.H. *et al.* (2009) High consistency of regional cortical thinning in aging across multiple samples. *Cereb. Cortex*, **19**, 2001–2012.
Fjell, A.M., Walhovd, K.B., Westlye, L.T., Østby, Y., Tamnes, C.K., Jernigan, T.L., Gamst, A. & Dale, A.M. (2010) When does brain aging accelerate? Dangers of quadratic fits in cross-sectional studies. *NeuroImage*, **50**, 1376–1383.
Fjell, A.M., Westlye, L.T., Grydeland, H., Amlien, I., Espeseth, T., Reinvang, I., Raz, N., Holland, D. *et al.* (2013) Critical ages in the life course of the adult brain: nonlinear subcortical aging. *Neurobiol. Aging*, **34**, 2239–2247.
Fletcher, M.A., Low, K.A., Boyd, R., Zimmerman, B., Gordon, B.A., Tan, C.H., Schneider-Garces, N., Sutton, B.P. *et al.* (2016) Comparing aging and fitness effects on brain anatomy. *Front. Hum. Neurosci.*, **10**, 286.
Fortin, J.-P., Cullen, N., Sheline, Y.I., Taylor, W.D., Aselcioglu, I., Cook, P.A., Adams, P., Cooper, C. *et al.* (2018) Harmonization of cortical thickness measurements across scanners and sites. *NeuroImage*, **167**, 104–120.
Fox, J. (2000) *Nonparametric Simple Regression: Smoothing Scatterplots*. Sage, Thousand Oaks, CA.
Franke, K. & Gaser, C. (2012) Longitudinal changes in individual BrainAGE in healthy aging, mild cognitive impairment, and Alzheimer's disease. *GeroPsych*, **25**, 235–245.
Franke, K., Ziegler, G., Klöppel, S. & Gaser, C. (2010) Estimating the age of healthy subjects from T1-weighted MRI scans using kernel methods: exploring the influence of various parameters. *NeuroImage*, **50**, 883–892.
Franke, K., Ristow, M. & Gaser, C. (2014) Gender-specific impact of personal health parameters on individual brain aging in cognitively unimpaired elderly subjects. *Front. Aging Neurosci.*, **6**, 94.
Free, S.L., Sisodiya, S.M., Cook, M.J., Fish, D.R. & Shorvon, S.D. (1996) Three-dimensional fractal analysis of the white matter surface from magnetic resonance images of the human brain. *Cereb. Cortex*, **6**, 830–836.
Freeman, S.H., Kandel, R., Cruz, L., Rozkalne, A., Newell, K., Frosch, M.P., Hedley-Whyte, E.T., Locascio, J.J. *et al.* (2008) Preservation of neuronal number despite age-related cortical brain atrophy in elderly subjects without Alzheimer disease. *J. Neuropath. Exp. Neur.*, **67**, 1205–1212.
Gao, J., Kwan, P.W. & Shi, D. (2010) Sparse kernel learning with LASSO and Bayesian inference algorithm. *Neural Networks*, **23**, 257–264.
Geerligs, L. & Tsvetanov, K.A. (2016) The use of resting state data in an integrative approach to studying neurocognitive ageing – commentary on Campbell and Schacter (2016). *Lang. Cogn. Neurosci.*, **32**, 684–691.
Gefen, T., Peterson, M., Papastefan, S.T., Martersteck, A., Whitney, K., Rademaker, A., Bigio, E.H., Weintraub, S. *et al.* (2015) Morphometric and histologic substrates of cingulate integrity in elders with exceptional memory capacity. *J. Neurosci.*, **35**, 1781–1791.
Gerrits, N.J.H.M., van Loenhoud, A.C., van den Berg, S.F., Berendse, H.W., Foncke, E.M.J., Klein, M., Stoffers, D., van der Werf, Y.D. *et al.* (2016) Cortical thickness, surface area and subcortical volume differentially contribute to cognitive heterogeneity in Parkinson's disease. *PLoS One*, **11**, e0148852.
Ghadery, C., Pirpamer, L., Hofer, E., Langkammer, C., Petrovic, K., Loitfelder, M., Schwingenschuh, P., Seiler, S. *et al.* (2015) R2* mapping for brain iron: associations with cognition in normal aging. *Neurobiol. Aging*, **36**, 925–932.
Gignac, G.E. & Bates, T.C. (2017) Brain volume and intelligence: the moderating role of intelligence measurement quality. *Intelligence*, **64**, 18–29.
Glatard, T., Lewis, L.B., da Silva, R.F., Adalat, R., Beck, N., Lepage, C., Rioux, P., Rousseau, M.-E. *et al.* (2015) Reproducibility of neuroimaging analyses across operating systems. *Front Neuroinform.*, **9**, 12.
Golbraikh, A. & Tropsha, A. (2002) Beware of q^2!. *J. Mol. Graph Model.*, **20**, 269–276.
Gronenschild, E.H.B.M., Habets, P., Jacobs, H.I.L., Mengelers, R., Rozendaal, N., van Os, J. & Marcelis, M. (2012) The effects of FreeSurfer version, workstation type, and Macintosh operating system version on anatomical volume and cortical thickness measurements. *PLoS One*, **7**, e38234.
Gunning-Dixon, F.M., Brickman, A.M., Cheng, J.C. & Alexopoulos, G.S. (2009) Aging of cerebral white matter: a review of MRI findings. *Int. J. Geriatr. Psych.*, **24**, 109–117.
Hagemann, G., Ugur, T., Schleussner, E., Mentzel, H.-J., Fitzek, C., Witte, O.W. & Gaser, C. (2011) Changes in brain size during the menstrual cycle. *PLoS One*, **6**, e14655.
Hagmann, P., Cammoun, L., Gigandet, X., Meuli, R., Honey, C.J., Wedeen, V.J. & Sporns, O. (2008) Mapping the structural core of human cerebral cortex. *PLoS Biol.*, **6**, e159.
Han, X., Jovicich, J., Salat, D., van der Kouwe, A., Quinn, B., Czanner, S., Busa, E., Pacheco, J. *et al.* (2006) Reliability of MRI-derived measurements of human cerebral cortical thickness: the effects of field strength, scanner upgrade and manufacturer. *NeuroImage*, **32**, 180–194.
Hänggi, J., Brütsch, K., Siegel, A.M. & Jäncke, L. (2014) The architecture of the chess player's brain. *Neuropsychologia*, **62**, 152–162.
Hanson, J.L., Hair, N., Shen, D.G., Shi, F., Gilmore, J.H., Wolfe, B.L. & Pollak, S.D. (2013) Family poverty affects the rate of human infant brain growth. *PLoS One*, **8**, e80954.
Hao, J., Rapp, P.R., Janssen, W.G.M., Lou, W., Lasley, B.L., Hof, P.R. & Morrison, J.H. (2007) Interactive effects of age and estrogen on cognition and pyramidal neurons in monkey prefrontal cortex. *Proc. Natl. Acad. Sci. USA*, **104**, 11465–11470.

Harrisberger, F., Spalek, K., Smieskova, R., Schmidt, A., Coynel, D., Milnik, A., Fastenrath, M., Freytag, V. *et al.* (2014) The association of the BDNF Val66Met polymorphism and the hippocampal volumes in healthy humans: a joint meta-analysis of published and new data. *Neurosci. Biobehav. Rev.*, **42**, 267–278.

Hastie, T., Tibshirani, R. & Friedman, J. (2009) *The Elements of Statistical Learning*. Springer, New York.

Hayes, S.M., Alosco, M.L. & Forman, D.E. (2014) The effects of aerobic exercise on cognitive and neural decline in aging and cardiovascular disease. *Curr. Geriatr. Rep.*, **3**, 282–290.

Herron, T.J., Kang, X. & Woods, D.L. (2015) Sex differences in cortical and subcortical human brain anatomy. *F1000Research*, **4**, 88.

van den Heuvel, M.P., Scholtens, L.H., Barrett, L.F., Hilgetag, C.C. & de Reus, M.A. (2015) Bridging cytoarchitectonics and connectomics in human cerebral cortex. *J. Neurosci.*, **35**, 13943–13948.

Hofman, M.A. (1991) The fractal geometry of convoluted brains. *J. Hirnforsch.*, **32**, 103–111.

Hogstrom, L.J., Westlye, L.T., Walhovd, K.B. & Fjell, A.M. (2013) The structure of the cerebral cortex across adult life: age-related patterns of surface area, thickness, and gyrification. *Cereb. Cortex*, **23**, 2521–2530.

Holmes, A.J., Hollinshead, M.O., Roffman, J.L., Smoller, J.W. & Buckner, R.L. (2016) Individual differences in cognitive control circuit anatomy link sensation seeking, impulsivity, and substance use. *J. Neurosci.*, **36**, 4038–4049.

Honea, R.A., Swerdlow, R.H., Vidoni, E.D., Goodwin, J. & Burns, J.M. (2010) Reduced gray matter volume in normal adults with a maternal family history of Alzheimer disease. *Neurology*, **74**, 113–120.

Hutton, C., Draganski, B., Ashburner, J. & Weiskopf, N. (2009) A comparison between voxel-based cortical thickness and voxel-based morphometry in normal aging. *NeuroImage*, **48**, 371–380.

Hyndman, R.J. & Koehler, A.B. (2006) Another look at measures of forecast accuracy. *Int. J. Forecasting*, **22**, 679–688.

Irimia, A., Torgerson, C.M., Goh, S.-Y.M. & Horn, J.D.V. (2015) Statistical estimation of physiological brain age as a descriptor of senescence rate during adulthood. *Brain Imaging Behav.*, **9**, 678–689.

Iscan, Z., Jin, T.B., Kendrick, A., Szeglin, B., Lu, H., Trivedi, M., Fava, M., McGrath, P.J. *et al.* (2015) Test-retest reliability of freesurfer measurements within and between sites: effects of visual approval process. *Hum. Brain Mapp.*, **36**, 3472–3485.

Jamil, T. & ter Braak, C.J.F. (2012) Selection properties of type II maximum likelihood (empirical Bayes) in linear models with individual variance components for predictors. *Pattern Recogn. Lett.*, **33**, 1205–1212.

Jernigan, T.L., Archibald, S.L., Fennema-Notestine, C., Gamst, A.C., Stout, J.C., Bonner, J. & Hesselink, J.R. (2001) Effects of age on tissues and regions of the cerebrum and cerebellum. *Neurobiol. Aging*, **22**, 581–594.

Jockwitz, C., Caspers, S., Lux, S., Jütten, K., Schleicher, A., Eickhoff, S.B., Amunts, K. & Zilles, K. (2017) Age- and function-related regional changes in cortical folding of the default mode network in older adults. *Brain Struct. Funct.*, **222**, 83–99.

Johnson, E.B., Gregory, S., Johnson, H.J., Durr, A., Leavitt, B.R., Roos, R.A., Rees, G., Tabrizi, S.J. *et al.* (2017) Recommendations for the use of automated gray matter segmentation tools: evidence from Huntington's disease. *Front. Neurol.*, **8**, 519.

Jovicich, J., Czanner, S., Han, X., Salat, D., van der Kouwe, A., Quinn, B., Pacheco, J., Albert, M. *et al.* (2009) MRI-derived measurements of human subcortical, ventricular and intracranial brain volumes: reliability effects of scan sessions, acquisition sequences, data analyses, scanner upgrade, scanner vendors and field strengths. *NeuroImage*, **46**, 177–192.

Jovicich, J., Marizzoni, M., Sala-Llonch, R., Bosch, B., Bartrés-Faz, D., Arnold, J., Benninghoff, J., Wiltfang, J. *et al.* (2013) Brain morphometry reproducibility in multi-center 3T MRI studies: a comparison of cross-sectional and longitudinal segmentations. *NeuroImage*, **83**, 472–484.

Kempton, M.J., Ettinger, U., Schmechtig, A., Winter, E.M., Smith, L., McMorris, T., Wilkinson, I.D., Williams, S.C.R. *et al.* (2009) Effects of acute dehydration on brain morphology in healthy humans. *Hum. Brain Mapp.*, **30**, 291–298.

Kennedy, K.M., Rodrigue, K.M., Bischof, G.N., Hebrank, A.C., Reuter-Lorenz, P.A. & Park, D.C. (2015) Age trajectories of functional activation under conditions of low and high processing demands: an adult lifespan fMRI study of the aging brain. *NeuroImage*, **104**, 21–34.

Kennedy, D.N., Haselgrove, C., Riehl, J., Preuss, N. & Buccigrossi, R. (2016) The NITRC image repository. *NeuroImage*, **124**, 1069–1073.

Khan, N.A., Baym, C.L., Monti, J.M., Raine, L.B., Drollette, E.S., Scudder, M.R., Moore, R.D., Kramer, A.F. *et al.* (2015) Central adiposity is negatively associated with hippocampal-dependent relational memory among overweight and obese children. *J. Pediatr.*, **166**, 302–308.

Kievit, R.A., Davis, S.W., Mitchell, D.J., Taylor, J.R., Duncan, J., Tyler, L.K., Brayne, C., Bullmore, E. *et al.* (2014) Distinct aspects of frontal lobe structure mediate age-related differences in fluid intelligence and multitasking. *Nat. Commun.*, **5**, 5658.

King, R.D., George, A.T., Jeon, T., Hynan, L.S., Youn, T.S., Kennedy, D.N. & Dickerson, B. (2009) Characterization of atrophic changes in the cerebral cortex using fractal dimensional analysis. *Brain Imaging Behav.*, **3**, 154–166.

King, R.D., Brown, B., Hwang, M., Jeon, T. & George, A.T. (2010) Fractal dimension analysis of the cortical ribbon in mild Alzheimer's disease. *NeuroImage*, **53**, 471–479.

Klein, A. & Tourville, J. (2012) 101 labeled brain images and a consistent human cortical labeling protocol. *Front. Neurosci.*, **6**, 171.

Kochunov, P., Rogers, W., Mangin, J.-F. & Lancaster, J. (2012) A library of cortical morphology analysis tools to study development, aging and genetics of cerebral cortex. *Neuroinformatics*, **10**, 81–96.

Kodiweera, C., Alexander, A.L., Harezlak, J., McAllister, T.W. & Wu, Y.-C. (2016) Age effects and sex differences in human brain white matter of young to middle-aged adults: a DTI, NODDI, and q-space study. *NeuroImage*, **128**, 180–192.

Koo, B.-B., Schettler, S.P., Murray, D.E., Lee, J.-M., Killiany, R.J., Rosene, D.L., Kim, D.-S. & Ronen, I. (2012) Age-related effects on cortical thickness patterns of the Rhesus monkey brain. *Neurobiol. Aging*, **33**, 200.

van der Kouwe, A.J.W., Benner, T., Salat, D.H. & Fischl, B. (2008) Brain morphometry with multiecho MPRAGE. *NeuroImage*, **40**, 559–569.

Kühn, S., Gleich, T., Lorenz, R.C., Lindenberger, U. & Gallinat, J. (2013) Playing Super Mario induces structural brain plasticity: gray matter changes resulting from training with a commercial video game. *Mol. Psychiatr.*, **19**, 265–271.

Kullmann, S., Callaghan, M.F., Heni, M., Weiskopf, N., Scheffler, K., Häring, H.-U., Fritsche, A., Veit, R. *et al.* (2016) Specific white matter tissue microstructure changes associated with obesity. *NeuroImage*, **125**, 36–44.

Kuperberg, G.R., Broome, M.R., McGuire, P.K., David, A.S., Eddy, M., Ozawa, F., Goff, D., West, W.C. *et al.* (2003) Regionally localized thinning of the cerebral cortex in schizophrenia. *Arch. Gen. Psychiat.*, **60**, 878–888.

Lebel, C., Gee, M., Camicioli, R., Wieler, M., Martin, W. & Beaulieu, C. (2012) Diffusion tensor imaging of white matter tract evolution over the lifespan. *NeuroImage*, **60**, 340–352.

Lee, F.S., Heimer, H., Giedd, J.N., Lein, E.S., Šestan, N., Weinberger, D.R. & Casey, B.J. (2014) Adolescent mental health–Opportunity and obligation. *Science*, **346**, 547–549.

Lemaitre, H., Goldman, A.L., Sambataro, F., Verchinski, B.A., Meyer-Lindenberg, A., Weinberger, D.R. & Mattay, V.S. (2012) Normal age-related brain morphometric changes: nonuniformity across cortical thickness, surface area and gray matter volume? *Neurobiol. Aging*, **33**, 617.

LeWinn, K.Z., Sheridan, M.A., Keyes, K.M., Hamilton, A. & McLaughlin, K.A. (2017) Sample composition alters associations between age and brain structure. *Nat. Commun.*, **8**, 874.

Li, Q., Song, M., Xu, J., Qin, W., Yu, C. & Jiang, T. (2017) Cortical thickness development of human primary visual cortex related to the age of blindness onset. *Brain Imaging Behav.*, **11**, 1029–1036.

Liem, F., Varoquaux, G., Kynast, J., Beyer, F., Masouleh, S.K., Huntenburg, J.M., Lampe, L., Rahim, M. *et al.* (2017) Predicting brain-age from multimodal imaging data captures cognitive impairment. *NeuroImage*, **148**, 179–188.

Lisofsky, N., Mårtensson, J., Eckert, A., Lindenberger, U., Gallinat, J. & Kühn, S. (2015) Hippocampal volume and functional connectivity changes during the female menstrual cycle. *NeuroImage*, **118**, 154–162.

Lo, A., Chernoff, H., Zheng, T. & Lo, S.-H. (2015) Why significant variables aren't automatically good predictors. *Proc. Natl. Acad. Sci. USA*, **112**, 13892–13897.

Luders, E., Cherbuin, N. & Gaser, C. (2016) Estimating brain age using high-resolution pattern recognition: younger brains in long-term meditation practitioners. *NeuroImage*, **134**, 508–513.

Lüsebrink, F., Wollrab, A. & Speck, O. (2013) Cortical thickness determination of the human brain using high resolution 3T and 7T MRI data. *NeuroImage*, **70**, 122–131.

MacKay, D.J.C. (1996) Bayesian non-linear modeling for the prediction competition. In Heidbreder, G.R. (Ed.), *Maximum Entropy and Bayesian Methods*. Springer, Dordrecht, pp. 221–234.

Madan, C.R. (2015) Creating 3D visualizations of MRI data: a brief guide. *F1000Research*, **4**, 466.

Madan, C.R. (2016) Prism: multiple spline regression with regularization, dimensionality reduction, and feature selection. *J. Open Source Softw.*, **1**, 31.

Madan, C.R. (2017) Advances in studying brain morphology: the benefits of open-access data. *Front. Hum. Neurosci.*, **11**, 405.
Madan, C.R. (2018) Shape-related characteristics of age-related differences in subcortical structures. *Aging Ment. Health*.
Madan, C.R. & Kensinger, E.A. (2016) Cortical complexity as a measure of age-related brain atrophy. *NeuroImage*, **134**, 617–629.
Madan, C.R. & Kensinger, E.A. (2017a) Age-related differences in the structural complexity of subcortical and ventricular structures. *Neurobiol. Aging*, **50**, 87–95.
Madan, C.R. & Kensinger, E.A. (2017b) Test–retest reliability of brain morphology estimates. *Brain Inform.*, **4**, 107–121.
Madsen, S.K., Steeg, G.V., Daianu, M., Mezher, A., Jahanshad, N., Nir, T.M., Hua, X., Gutman, B.A. *et al.* (2016) Relative value of diverse brain MRI and blood-based biomarkers for predicting cognitive decline in the elderly. In Styner, M.A. & Angelini, E.D. (Eds), *Medical Imaging 2016: Image Processing* 978411. SPIE, Orlando, FL.
Magnotta, V.A., Andreasen, N.C., Schultz, S.K., Harris, G., Cizadlo, T., Heckel, D., Nopoulos, P. & Flaum, M. (1999) Quantitative *in vivo* measurement of gyrification in the human brain: changes associated with aging. *Cereb. Cortex*, **9**, 151–160.
Maguire, E.A., Gadian, D.G., Johnsrude, I.S., Good, C.D., Ashburner, J., Frackowiak, R.S.J. & Frith, C.D. (2000) Navigation-related structural change in the hippocampi of taxi drivers. *Proc. Natl. Acad. Sci. USA*, **97**, 4398–4403.
Mandelbrot, B.B. (1967) How long is the coast of Britain? Statistical self-similarity and fractional dimension. *Science*, **156**, 636–638.
Marcus, D.S., Wang, T.H., Parker, J., Csernansky, J.G., Morris, J.C. & Buckner, R.L. (2007) Open Access Series of Imaging Studies (OASIS): cross-sectional MRI data in young, middle aged, nondemented, and demented older adults. *J. Cognit. Neurosci.*, **19**, 1498–1507.
May, A. (2011) Experience-dependent structural plasticity in the adult human brain. *Trends Cogn. Sci.*, **15**, 475–482.
McKay, D.R., Knowles, E.E.M., Winkler, A.A.M., Sprooten, E., Kochunov, P., Olvera, R.L., Curran, J.E., Kent, J.W. *et al.* (2014) Influence of age, sex and genetic factors on the human brain. *Brain Imaging Behav.*, **8**, 143–152.
Mechelli, A., Price, C., Friston, K. & Ashburner, J. (2005) Voxel-based morphometry of the human brain: methods and applications. *Curr. Med. Imaging Rev.*, **1**, 105–113.
Mennes, M., Biswal, B.B., Castellanos, F.X. & Milham, M.P. (2013) Making data sharing work: the FCP/INDI experience. *NeuroImage*, **82**, 683–691.
Meyer, M., Liem, F., Hirsiger, S., Jancke, L. & Hanggi, J. (2014) Cortical surface area and cortical thickness demonstrate differential structural asymmetry in auditory-related areas of the human cortex. *Cereb. Cortex*, **24**, 2541–2552.
Meyers, S.M., Tam, R., Lee, J.S., Kolind, S.H., Vavasour, I.M., Mackie, E., Zhao, Y., Laule, C. *et al.* (2016) Does hydration status affect MRI measures of brain volume or water content? *J. Magn. Reson. Imaging*, **44**, 296–304.
Mills, K.L., Goddings, A.-L., Herting, M.M., Meuwese, R., Blakemore, S.-J., Crone, E.A., Dahl, R.E., Güroğlu, B. *et al.* (2016) Structural brain development between childhood and adulthood: convergence across four longitudinal samples. *NeuroImage*, **141**, 273–281.
Mormino, E.C., Betensky, R.A., Hedden, T., Schultz, A.P., Ward, A., Huijbers, W., Rentz, D.M., Johnson, K.A. *et al.* (2014) Amyloid and APOE $\in$4 interact to influence short-term decline in preclinical Alzheimer disease. *Neurology*, **82**, 1760–1767.
Morrison, J.H. & Baxter, M.G. (2012) The ageing cortical synapse: Hallmarks and implications for cognitive decline. *Nat. Rev. Neurosci.*, **13**, 240–250.
Morrison, J.H. & Hof, P.R. (1997) Life and death of neurons in the aging brain. *Science*, **278**, 412–419.
Nakamura, K., Brown, R.A., Araujo, D., Narayanan, S. & Arnold, D.L. (2014) Correlation between brain volume change and T2 relaxation time induced by dehydration and rehydration: implications for monitoring atrophy in clinical studies. *Neuroimage Clin.*, **6**, 166–170.
Nakamura, K., Brown, R.A., Narayanan, S., Collins, D.L. & Arnold, D.L. (2015) Diurnal fluctuations in brain volume: statistical analyses of MRI from large populations. *NeuroImage*, **118**, 126–132.
Nemoto, K., Ohnishi, T., Mori, T., Moriguchi, Y., Hashimoto, R., Asada, T. & Kunugi, H. (2006) The Val66Met polymorphism of the brain-derived neurotrophic factor gene affects age-related brain morphology. *Neurosci. Lett.*, **397**, 25–29.
Nenadic, I., Yotter, R.A., Sauer, H. & Gaser, C. (2014) Cortical surface complexity in frontal and temporal areas varies across subgroups of schizophrenia. *Hum. Brain Mapp.*, **35**, 1691–1699.
Okonkwo, O.C., Xu, G., Dowling, N.M., Bendlin, B.B., LaRue, A., Hermann, B.P., Koscik, R., Jonaitis, E. *et al.* (2012) Family history of Alzheimer disease predicts hippocampal atrophy in healthy middle-aged adults. *Neurology*, **78**, 1769–1776.
Ossewaarde, L., van Wingen, G.A., Rijpkema, M., Bäckström, T., Hermans, E.J. & Fernández, G. (2013) Menstrual cycle-related changes in amygdala morphology are associated with changes in stress sensitivity. *Hum. Brain Mapp.*, **34**, 1187–1193.
Palaniyappan, L. & Liddle, P.F. (2012) Differential effects of surface area, gyrification and cortical thickness on voxel based morphometric deficits in schizophrenia. *NeuroImage*, **60**, 693–699.
Pardoe, H.R., Hiess, R.K. & Kuzniecky, R. (2016) Motion and morphometry in clinical and nonclinical populations. *NeuroImage*, **135**, 177–185.
Park, T. & Casella, G. (2008) The Bayesian Lasso. *J. Am. Stat. Assoc.*, **103**, 681–686.
Peters, A. (2002) Structural changes that occur during normal aging of primate cerebral hemispheres. *Neurosci. Biobehav. Rev.*, **26**, 733–741.
Peters, A. & Rosene, D.L. (2003) In aging, is it gray or white? *J. Comp. Neurol.*, **462**, 139–143.
Peters, A., Morrison, J.H., Rosene, D.L. & Hyman, B.T. (1998) Are neurons lost from the primate cerebral cortex during normal aging? *Cereb. Cortex*, **8**, 295–300.
Pezawas, L., Verchinski, B.A., Mattay, V.S., Callicott, J.H., Kolachana, B.S., Straub, R.E., Egan, M.F., Meyer-Lindenberg, A. *et al.* (2004) The brain-derived neurotrophic factor Val66Met polymorphism and variation in human cortical morphology. *J. Neurosci.*, **24**, 10099–10102.
Pfefferbaum, A. & Sullivan, E.V. (2015) Cross-sectional versus longitudinal estimates of age-related changes in the adult brain: overlaps and discrepancies. *Neurobiol. Aging*, **36**, 2563–2567.
Piccolo, L.R., Merz, E.C., He, X., Sowell, E.R. & Noble, K.G. (2016) Age-related differences in cortical thickness vary by socioeconomic status. *PLoS One*, **11**, e0162511.
Poldrack, R.A. & Gorgolewski, K.J. (2014) Making big data open: data sharing in neuroimaging. *Nat. Neurosci.*, **17**, 1510–1517.
Poldrack, R.A., Baker, C.I., Durnez, J., Gorgolewski, K.J., Matthews, P.M., Munafò, M.R., Nichols, T.E., Poline, J.-B. *et al.* (2017) Scanning the horizon: towards transparent and reproducible neuroimaging research. *Nat. Rev. Neurosci.*, **18**, 115–126.
Potvin, O., Mouiha, A., Dieumegarde, L. & Duchesne, S. (2016) Normative data for subcortical regional volumes over the lifetime of the adult human brain. *NeuroImage*, **137**, 9–20.
Protopopescu, X., Butler, T., Pan, H., Root, J., Altemus, M., Polanecsky, M., McEwen, B., Silbersweig, D. *et al.* (2008) Hippocampal structural changes across the menstrual cycle. *Hippocampus*, **18**, 985–988.
Qin, J., Chen, S.-G., Hu, D., Zeng, L.-L., Fan, Y.-M., Chen, X.-P. & Shen, H. (2015) Predicting individual brain maturity using dynamic functional connectivity. *Front. Hum. Neurosci.*, **9**, 418.
Rao, R.B., Fung, G. & Rosales, R. (2008) *On the dangers of cross-validation. An experimental evaluation*. Proceedings of the 2008 SIAM International Conference on Data Mining Proceedings of the 2008 SIAM International Conference on Data Mining, pp. 588–596. SIAM.
Rasmussen, C.E. & Williams, C.K.I. (2006) *Gaussian Processes for Machine Learning*. MIT Press, Cambridge, MA.
Raz, N. & Rodrigue, K.M. (2006) Differential aging of the brain: patterns, cognitive correlates and modifiers. *Neurosci. Biobehav. Rev.*, **30**, 730–748.
Reagh, Z. & Yassa, M. (2017) Selective vulnerabilities and biomarkers in neurocognitive aging. *F1000Research*, **6**, 491.
Reinvang, I., Espeseth, T. & Westlye, L.T. (2013) APOE-related biomarker profiles in non-pathological aging and early phases of Alzheimer's disease. *Neurosci. Biobehav. Rev.*, **37**, 1322–1335.
Reuter, M., Tisdall, M.D., Qureshi, A., Buckner, R.L., van der Kouwe, A.J.W. & Fischl, B. (2015) Head motion during MRI acquisition reduces gray matter volume and thickness estimates. *NeuroImage*, **107**, 107–115.
Riccelli, R., Toschi, N., Nigro, S., Terracciano, A. & Passamonti, L. (2017) Surface-based morphometry reveals the neuroanatomical basis of the five-factor model of personality. *Soc. Cogn. Affect. Neurosci.*, **12**, 671–684.
Riedel, B.C., Thompson, P.M. & Brinton, R.D. (2016) Age, APOE and sex: triad of risk of Alzheimer's disease. *J. Steroid Biochemist. Mol. Biol.*, **160**, 134–147.
Rosas, H.D., Liu, A.K., Hersch, S., Glessner, M., Ferrante, R.J., Salat, D.H., van der Kouwe, A., Jenkins, B.G. *et al.* (2002) Regional and progressive

thinning of the cortical ribbon in Huntington's disease. *Neurology*, **58**, 695–701.
Saeb, S., Lonini, L., Jayaraman, A., Mohr, D.C. & Kording, K.P. (2016) Voodoo machine learning for clinical predictions. *bioRxiv*.
Salat, D.H. (2014) Diffusion tensor imaging in the study of aging and age-associated neural disease. In *Diffusion MRI: From Quantitative Measurement to In-vivo Neuroanatomy*. Elsevier, San Diego, CA, pp. 257–281.
Salat, D.H., Buckner, R.L., Snyder, A.Z., Greve, D.N., Desikan, R.S.R., Busa, E., Morris, J.C., Dale, A.M. *et al.* (2004) Thinning of the cerebral cortex in aging. *Cereb. Cortex*, **14**, 721–730.
Sandu, A.-L., Rasmussen, I.-A., Lundervold, A., Kreuder, F., Neckelmann, G., Hugdahl, K. & Specht, K. (2008) Fractal dimension analysis of MR images reveals grey matter structure irregularities in schizophrenia. *Comput. Med. Imaging Graph.*, **32**, 150–158.
Savalia, N.K., Agres, P.F., Chan, M.Y., Feczko, E.J., Kennedy, K.M. & Wig, G.S. (2017) Motion-related artifacts in structural brain images revealed with independent estimates of in-scanner head motion. *Hum. Brain Mapp.*, **38**, 472–492.
Schaer, M., Cuadra, M.B., Schmansky, N., Fischl, B., Thiran, J.-P. & Eliez, S. (2012) How to measure cortical folding from MR images: a step-by-step tutorial to compute local gyrification index. *J. Vis. Exp.*, **59**, e3417.
Scheibel, M.E., Lindsay, R.D., Tomiyasu, U. & Scheibel, A.B. (1975) Progressive dendritic changes in aging human cortex. *Exp. Neurol.*, **47**, 392–403.
Schlaffke, L., Lissek, S., Lenz, M., Brüne, M., Juckel, G., Hinrichs, T., Platen, P., Tegenthoff, M. *et al.* (2014) Sports and brain morphology – A voxel-based morphometry study with endurance athletes and martial artists. *Neuroscience*, **259**, 35–42.
Schnack, H.G., van Haren, N.E.M., Nieuwenhuis, M., Pol, H.E.H., Cahn, W. & Kahn, R.S. (2016) Accelerated brain aging in schizophrenia: a longitudinal pattern recognition study. *Am. J. Psychiatry*, **173**, 607–616.
Scholtens, L.H., de Reus, M.A. & van den Heuvel, M.P. (2015) Linking contemporary high resolution magnetic resonance imaging to the von Economo legacy: a study on the comparison of MRI cortical thickness and histological measurements of cortical structure. *Hum. Brain Mapp.*, **36**, 3038–3046.
Scholtens, L.H., de Reus, M.A., de Lange, S.C., Schmidt, R. & van den Heuvel, M.P. (2018) An MRI von Economo–Koskinas atlas. *NeuroImage*.
Shenkin, S.D., Pernet, C., Nichols, T.E., Poline, J.-B., Matthews, P.M., van der Lugt, A., Mackay, C., Lanyon, L. *et al.* (2017) Improving data availability for brain image biobanking in healthy subjects: practice-based suggestions from an international multidisciplinary working group. *NeuroImage*, **153**, 399–409.
Skocik, M., Collins, J., Callahan-Flintoft, C., Bowman, H. & Wyble, B. (2016) I tried a bunch of things: The dangers of unexpected overfitting in classification. *bioRxiv*.
Somerville, L.H. (2016) Searching for signatures of brain maturity: what are we searching for? *Neuron*, **92**, 1164–1167.
Sowell, E.R., Peterson, B.S., Kan, E., Woods, R.P., Yoshii, J., Bansal, R., Xu, D., Zhu, H., Thompson, P.M. & Toga, A.W. (2007) Sex differences in cortical thickness mapped in 176 healthy individuals between 7 and 87 years of age. *Cereb. Cortex*, **17**, 1550–1560.
Sowell, E.R., Peterson, B.S., Thompson, P.M., Welcome, S.E., Henkenius, A.L. & Toga, A.W. (2003) Mapping cortical change across the human life span. *Nat. Neurosci.*, **6**, 309–315.
Stark, S.M., Yassa, M.A., Lacy, J.W. & Stark, C.E.L. (2013) A task to assess behavioral pattern separation (BPS) in humans: data from healthy aging and mild cognitive impairment. *Neuropsychologia*, **51**, 2442–2449.
Steffener, J., Habeck, C., OShea, D., Razlighi, Q., Bherer, L. & Stern, Y. (2016) Differences between chronological and brain age are related to education and self-reported physical activity. *Neurobiol. Aging*, **40**, 138–144.
Streitbürger, D.-P., Möller, H.E., Tittgemeyer, M., Hund-Georgiadis, M., Schroeter, M.L. & Mueller, K. (2012) Investigating structural brain changes of dehydration using voxel-based morphometry. *PLoS One*, **7**, e44195.
Strike, L.T., Couvy-Duchesne, B., Hansell, N.K., Cuellar-Partida, G., Medland, S.E. & Wright, M.J. (2015) Genetics and brain morphology. *Neuropsychol. Rev.*, **25**, 63–96.
Strømmen, K., Blakstad, E.W., Moltu, S.J., Almaas, A.N., Westerberg, A.C., Amlien, I.K., Rønnestad, A.E., Nakstad, B. *et al.* (2015) Enhanced nutrient supply to very low birth weight infants is associated with improved white matter maturation and head growth. *Neonatology*, **107**, 68–75.
Tang, Y.-Y., Hölzel, B.K. & Posner, M.I. (2015) The neuroscience of mindfulness meditation. *Nat. Rev. Neurosci.*, **16**, 213–225.
Teipel, S.J., Lerche, M., Kilimann, I., O'Brien, K., Grothe, M., Meyer, P., Li, X., Sänger, P. *et al.* (2014) Decline of fiber tract integrity over the adult age range: a diffusion spectrum imaging study. *J. Magn. Reson. Imaging*, **40**, 348–359.
Terry, R.D., DeTeresa, R. & Hansen, L.A. (1987) Neocortical cell counts in normal human adult aging. *Ann. Neurol.*, **21**, 530–539.
Tervaniemi, M. (2009) Musicians-same or different?. *Ann. N.Y. Acad. Sci.*, **1169**, 151–156.
Thompson, P.M., Lee, A.D., Dutton, R.A., Geaga, J.A., Hayashi, K.M., Eckert, M.A., Bellugi, U., Galaburda, A.M. *et al.* (2005) Abnormal cortical complexity and thickness profiles mapped in Williams syndrome. *J. Neurosci.*, **25**, 4146–4158.
Tibshirani, R. (1996) Regression shrinkage and selection via the LASSO. *J. Roy Stat. Soc. B*, **58**, 267–288.
Tipping, M.E. (2000) The relevance vector machine. *Adv. Neural. Inf. Process. Syst.*, **12**, 652–658.
Tipping, M.E. (2001) Sparse Bayesian learning and the relevance vector machine. *J. Mach. Learn. Res.*, **1**, 211–244.
Tipping, M.E. & Faul, A.C. (2003) Fast marginal likelihood maximisation for sparse Bayesian models. Proceedings of the Ninth International Workshop on Artificial Intelligence and Statistics (AISTATS).
Toro, R., Perron, M., Pike, B., Richer, L., Veillette, S., Pausova, Z. & Paus, T. (2008) Brain size and folding of the human cerebral cortex. *Cereb. Cortex*, **18**, 2352–2357.
Trefler, A., Sadeghi, N., Thomas, A.G., Pierpaoli, C., Baker, C.I. & Thomas, C. (2016) Impact of time-of-day on brain morphometric measures derived from T1-weighted magnetic resonance imaging. *NeuroImage*, **133**, 41–52.
Tseng, B.Y., Uh, J., Rossetti, H.C., Cullum, C.M., Diaz-Arrastia, R.F., Levine, B.D., Lu, H. & Zhang, R. (2013) Masters athletes exhibit larger regional brain volume and better cognitive performance than sedentary older adults. *J. Magn. Reson. Imaging*, **38**, 1169–1176.
Uylings, H.B.M. & de Brabander, J.M. (2002) Neuronal changes in normal human aging and Alzheimer's disease. *Brain Cogn.*, **49**, 268–276.
Valk, S.L., Bernhardt, B.C., Trautwein, F.-M., Böckler, A., Kanske, P., Guizard, N., Collins, D.L. & Singer, T. (2017) Structural plasticity of the social brain: differential change after socio-affective and cognitive mental training. *Sci. Adv.*, **3**, e1700489.
Van Dijk, K.R.A., Sabuncu, M.R. & Buckner, R.L. (2012) The influence of head motion on intrinsic functional connectivity MRI. *NeuroImage*, **59**, 431–438.
Wahba, G. (1990) *Spline Models for Observational Data*. Society for Industrial and Applied Mathematics, Philadelphia, PA.
Wahba, G. & Wold, S. (1975) A completely automatic French curve: fitting spline functions by cross validation. *Commun. Stat. A-Theor.*, **4**, 1–17.
Walhovd, K.B., Westlye, L.T., Amlien, I., Espeseth, T., Reinvang, I., Raz, N., Agartz, I., Salat, D.H. *et al.* (2011) Consistent neuroanatomical age-related volume differences across multiple samples. *Neurobiol. Aging*, **32**, 916–932.
Walhovd, K.B., Fjell, A.M., Brown, T.T., Kuperman, J.M., Chung, Y., Hagler, D.J., Roddey, J.C., Erhart, M. *et al.* (2012) Long-term influence of normal variation in neonatal characteristics on human brain development. *Proc. Natl. Acad. Sci. USA*, **109**, 20089–20094.
Walhovd, K.B., Tamnes, C.K. & Fjell, A.M. (2014) Brain structural maturation and the foundations of cognitive behavioral development. *Curr. Opin. Neurol.*, **27**, 176–184.
Walhovd, K.B., Krogsrud, S.K., Amlien, I.K., Bartsch, H., Bjørnerud, A., Due-Tønnessen, P., Grydeland, H., Hagler, D.J. *et al.* (2016) Neurodevelopmental origins of lifespan changes in brain and cognition. *Proc. Natl. Acad. Sci. USA*, **113**, 9357–9362.
Wang, Y., Necus, J., Kaiser, M. & Mota, B. (2016) Universality in human cortical folding in health and disease. *Proc. Natl. Acad. Sci. USA*, **113**, 12820–12825.
Ward, R.J., Zucca, F.A., Duyn, J.H., Crichton, R.R. & Zecca, L. (2014) The role of iron in brain ageing and neurodegenerative disorders. *Lancet Neurol.*, **13**, 1045–1060.
Williams, V.J., Hayes, J.P., Forman, D.E., Salat, D.H., Sperling, R.A., Verfaellie, M. & Hayes, S.M. (2017) Cardiorespiratory fitness is differentially associated with cortical thickness in young and older adults. *NeuroImage*, **146**, 1084–1092.
Wipf, D.P. & Nagarajan, S.S. (2007) A new view of automatic relevance determination. *Adv. Neural. Inf. Process. Syst.*, **20**, 1625–1632.
Wonderlick, J.S., Ziegler, D.A., Hosseini-Varnamkhasti, P., Locascio, J.J., Bakkour, A., van der Kouwe, A., Triantafyllou, C., Corkin, S. *et al.* (2009) Reliability of MRI-derived cortical and subcortical morphometric measures: effects of pulse sequence, voxel geometry, and parallel imaging. *NeuroImage*, **44**, 1324–1333.

Wu, Y.-T., Shyu, K.-K., Jao, C.-W., Wang, Z.-Y., Soong, B.-W., Wu, H.-M. & Wang, P.-S. (2010) Fractal dimension analysis for quantifying cerebellar morphological change of multiple system atrophy of the cerebellar type (MSA-C). *NeuroImage*, **49**, 539–551.

Yamagishi, T., Takagishi, H., de Souza Rodrigues Fermin, A., Kanai, R., Li, Y. & Matsumoto, Y. (2016) Cortical thickness of the dorsolateral prefrontal cortex predicts strategic choices in economic games. *Proc. Natl. Acad. Sci. USA*, **113**, 5582–5587.

Zaretskaya, N., Fischl, B., Reuter, M., Renvall, V. & Polimeni, J.R. (2018) Advantages of cortical surface reconstruction using submillimeter 7 T MEMPRAGE. *NeuroImage*, **165**, 11–26.

Zecca, L., Youdim, M.B.H., Riederer, P., Connor, J.R. & Crichton, R.R. (2004) Iron, brain ageing and neurodegenerative disorders. *Nat. Rev. Neurosci.*, **5**, 863–873.

Zilles, K. & Amunts, K. (2010) Centenary of Brodmanns map — conception and fate. *Nat. Rev. Neurosci.*, **11**, 139–145.

Zilles, K., Armstrong, E., Schleicher, A. & Kretschmann, H.-J. (1988) The human pattern of gyrification in the cerebral cortex. *Anat. Embryol.*, **179**, 173–179.

Zilles, K., Armstrong, E., Moser, K.H., Schleicher, A. & Stephan, H. (1989) Gyrification in the cerebral cortex of primates. *Brain Behav. Evol.*, **34**, 143–150.